

Efficient and accurate causal inference with hidden confounders from genome-transcriptome variation data

Lingfei Wang and Tom Michoel*

Division of Genetics and Genomics, The Roslin Institute, The University of Edinburgh, Easter Bush, Midlothian EH25 9RG, UK

Abstract

Mapping gene expression as a quantitative trait using whole genome-sequencing and transcriptome analysis allows to discover the functional consequences of genetic variation. We developed a novel method and ultra-fast software Findr for highly accurate causal inference between gene expression traits using cis-regulatory DNA variations as causal anchors, which improves current methods by taking into account hidden confounders and weak regulations. Findr outperformed existing methods on the DREAM5 Systems Genetics challenge and on the prediction of microRNA and transcription factor targets in human lymphoblastoid cells, while being nearly a million times faster. Findr is publicly available at <https://github.com/lingfeiwang/findr>.

Author summary

Understanding how genetic variation between individuals determines variation in observable traits or disease risk is one of the core aims of genetics. It is known that genetic variation often affects gene regulatory DNA elements and directly causes variation in expression of nearby genes. This effect in turn cascades down to other genes via the complex pathways and gene interaction networks that ultimately govern how cells operate in an ever changing environment. In theory, when genetic variation and gene expression levels are measured simultaneously in a large number of individuals, the causal effects of genes on each other can be inferred using statistical models similar to those used in randomized controlled trials. We developed a novel method and ultra-fast software Findr which, unlike existing methods, takes

*Corresponding author. Email: Tom.Michoel@roslin.ed.ac.uk

into account the complex but unknown network context when predicting causality between specific gene pairs. Findr’s predictions have a significantly higher overlap with known gene networks compared to existing methods, using both simulated and real data. Findr is also nearly a million times faster, and hence the only software in its class that can handle modern datasets where the expression levels of ten-thousands of genes are simultaneously measured in hundreds to thousands of individuals.

1 Introduction

Genetic variation in non-coding genomic regions, including at loci associated with complex traits and diseases identified by genome-wide association studies, predominantly plays a gene-regulatory role¹. Whole genome and transcriptome analysis of natural populations has therefore become a common practice to understand how genetic variation leads to variation in phenotypes². The number and size of studies mapping genome and transcriptome variation has surged in recent years due to the advent of high-throughput sequencing technologies, and ever more expansive catalogues of expression-associated DNA variants, termed expression quantitative trait loci (eQTLs), are being mapped in humans, model organisms, crops and other species^{1,3-5}. Unravelling the causal hierarchies between DNA variants and their associated genes and phenotypes is now the key challenge to enable the discovery of novel molecular mechanisms, disease biomarkers or candidate drug targets from this type of data^{6,7}.

It is believed that genetic variation can be used to infer the causal directions of regulation between coexpressed genes, based on the principle that genetic variation causes variation in nearby gene expression and acts as a causal anchor for identifying downstream genes^{8,9}. Although numerous statistical models have been proposed for causal inference with genotype and gene expression data from matching samples^{10,12,14,55,64,65}, no software implementation in the public domain is efficient enough to handle the volume of contemporary datasets, hindering any attempts to evaluate their performances. Moreover, existing statistical models rely on a conditional independence test which assumes that no hidden confounding factors affect the coexpression of causally related gene pairs. However gene regulatory networks are known to exhibit redundancy¹⁶ and are organized into higher order network motifs¹⁷, suggesting that confounding of causal relations by known or unknown common upstream regulators is the

rule rather than the exception. Moreover, it is also known that the conditional independence test is susceptible to variations in relative measurement errors between genes^{8,9}, an inherent feature of both microarray and RNA-seq based expression data¹⁸.

To investigate and address these issues, we developed Findr (Fast Inference of Networks from Directed Regulations), an ultra-fast software package that incorporates existing and novel statistical causal inference tests. The novel tests were designed to take into account the presence of unknown confounding effects, and were evaluated systematically against multiple existing methods using both simulated and real data.

2 Results

2.1 Findr incorporates existing and novel causal inference tests

Findr performs six likelihood ratio tests involving pairs of genes (or exons or transcripts) A , B , and an eQTL E of A (Table 1, Section 4.3). Findr then calculates Bayesian posterior probabilities of the hypothesis of interest being true based on the observed likelihood ratio test statistics (denoted P_i , $i = 0$ to 5, $0 \leq P_i \leq 1$, Section 4.5). For this purpose, Findr utilizes newly derived analytical formulae for the null distributions of the likelihood ratios of the implemented tests (Section 4.4, Figure S1). This, together with efficient programming, resulted in a dramatic speedup compared to the standard computationally expensive approach of generating random permutations. The six posterior probabilities are then combined into the traditional causal inference test, our new causal inference test, and separately a correlation test that does not incorporate genotype information (Section 4.6). Each of these tests verifies whether the data arose from a specific subset of (E, A, B) relations (Table 1) among the full hypothesis space of all their possible interactions, and results in a probability of a causal interaction $A \rightarrow B$ being true, which can be used to rank predictions according to significance or to reconstruct directed networks of gene regulations by keeping all interactions exceeding a probability threshold.

2.2 Traditional causal inference fails in the presence of hidden confounders and weak regulations

Findr’s computational speed allowed us to systematically evaluate traditional causal inference methods for the first time. We obtained five datasets with 999 samples simulated from synthetic gene regulatory networks of 1,000 genes with known genetic architecture from the DREAM5 Systems Genetics Challenge (Section 4.1), and subsampled each dataset to observe how performance depends on sample size (Section 4.7). The correlation test (P_0) does not incorporate genotype information and was used as a benchmark for performance evaluations in terms of areas under the receiver operating characteristic (AUROC) and precision-recall (AUPR) curves (Section 4.7). The traditional method⁵⁵ combines the secondary (P_2) and independence (P_3) tests sequentially (Table 1, Section 4.6), and was evaluated by comparing P_2 and P_2P_3 separately against the correlation test. Both the secondary test alone and the traditional causal inference test combination were found to underperform the correlation test (Figure 1A,B). Moreover, the inclusion of the conditional independence test worsened inference accuracy, more so with increasing sample size (Figure 1A,B) and increasing number of regulations per gene (Supplementary Material S2.3). Similar performance drops were also observed for the Causal Inference Test (CIT)^{64,65} software, which also is based on the conditional independence test (Figure S3).

We believe that the failure of traditional causal inference is due to an elevated false negative rate (FNR) coming from two sources. First, the secondary test is less powerful in identifying weak interactions than the correlation test. In a true regulation $E \rightarrow A \rightarrow B$, the secondary linkage ($E \rightarrow B$) is the result of two direct linkages chained together, and is harder to detect than either of them. The secondary test hence picks up fewer true regulations, and consequently has a higher FNR. Second, the conditional independence test is counter-productive in the presence of hidden confounders (i.e. common upstream regulators). In such cases, even if $E \rightarrow A \rightarrow B$ is genuine, the conditional independence test will find E and B to be still correlated after conditioning on A due to a collider effect (Figure S5)¹⁹. Hence the conditional independence test only reports positive on $E \rightarrow A \rightarrow B$ relations without confounder, further raising the FNR. This is supported by the observation of worsening performance with increasing sample size (where confounding effects become more distinguishable) and increasing

number of regulations per gene (which leads to more confounding).

To further support this claim, we examined the inference precision among the top predictions from the traditional test, separately for gene pairs directly unconfounded or confounded by at least one gene (Section 4.7). Compared to unconfounded gene pairs, confounded ones resulted in significantly more false positives among the top predictions (Figure 1C). Furthermore, the vast majority of real interactions fell outside the top 1% of predictions (i.e. had small posterior probability) [92% (651/706) for confounded and 86% (609/709) for unconfounded interactions, Figure 1C]. Together, these results again showed the failure of the traditional test on confounded interactions and its high false negative rate overall.

2.3 Findr accounts for weak secondary linkage, allows for hidden confounders, and outperforms existing methods on simulated data

To overcome the limitations of traditional causal inference methods, Findr incorporates two additional tests (Table 1 and Section 4.3). The relevance test (P_4) verifies that B is not independent from A and E simultaneously and is more sensitive for picking up weak secondary linkages than the secondary linkage test. The controlled test (P_5) ensures that the correlation between A and B cannot be fully explained by E , i.e. excludes pleiotropy. The same subsampling analysis revealed that P_4 performed best in terms of AUROC, and AUPR with small sample sizes, whilst the combination P_2P_5 achieved highest AUPR for larger sample sizes (Figure 1A,B). Most importantly, both tests consistently outperformed the correlation test (P_0), particularly for AUPR. This demonstrates conclusively in a comparative setting that the inclusion of genotype data indeed can improve regulatory network inference. These observations are consistent across all five DREAM datasets (Figure S2).

We combined the advantages of P_4 and P_2P_5 by averaging them in a composite test (P) (Section 4.6), which outperformed P_4 and P_2P_5 at all sample sizes (Figure 1 and Figure S2) and hence was appointed as Findr’s new test for causal inference. Findr’s new test (P) obtained consistently higher levels of local precision (i.e. one minus local FDR) on confounded and unconfounded gene pairs compared to Findr’s traditional causal inference test (P_T) (Figure 1C,D), and outperformed the traditional test (P_T), correlation test (P_0), CIT, and every participating method of the DREAM5 Systems Genetics Challenge (Section 4.1) in terms of

AUROC and AUPR on all 15 datasets (Figure 1E,F, Table S1, Figure S4).

Specifically, Findr’s new test was able to address the inflated FNR of the traditional method due to confounded interactions. It performed almost equally well on confounded and unconfounded gene pairs and, compared to the traditional test, significantly fewer real interactions fell outside the top 1% of predictions (55% vs. 92% for confounded and 45% vs. 86% for unconfounded interactions, Figure 1D, Figure S6).

2.4 The conditional independence test incurs false negatives for unconfounded regulations due to measurement error

The traditional causal inference method based on the conditional independence test results in false negatives for confounded interactions, whose effect was shown significant for the simulated DREAM datasets. However, the traditional test surprisingly reported more confounded gene pairs than the new test in its top predictions (albeit with lower precision), and correspondingly fewer unconfounded gene pairs (Figure 1C,D, Figure S6).

We hypothesized that this inconsistency originated from yet another source of false negatives, where measurement error can confuse the conditional independence test. Measurement error in an upstream variable (called A in Table 1) does not affect the expression levels of its downstream targets, and hence a more realistic model for gene regulation is $E \rightarrow A^{(t)} \rightarrow B$ with $A^{(t)} \rightarrow A$, where the measured quantities are E , A , and B , but the true value for A , noted $A^{(t)}$, remains unknown. When the measurement error (in $A^{(t)} \rightarrow A$) is significant, conditioning on A instead of $A^{(t)}$ cannot remove all the correlation between E and B and would therefore report false negatives for unconfounded interactions as well. This effect has been previously studied, for example in epidemiology as the “spurious appearance of odds-ratio heterogeneity”²⁰.

We verified our hypothesis with a simple simulation (Section 4.8). In a typical scenario with 300 samples from a monoallelic species, minor allele frequency 0.1, and a third of the total variance of B coming from $A^{(t)}$, the conditional independence test reported false negatives (likelihood ratio p-value $\ll 1$, i.e. rejecting the null hypothesis of conditional independence, cf. Table 1) as long as measurement error contributed more than half of A ’s total unexplained variance (Figure 2B). False negatives occurred at even weaker measurement errors, when the

sample sizes were larger or when stronger $A \rightarrow B$ regulations were assumed (Figure S7).

This observation goes beyond the well-known problems that arise from a large measurement error in all variables, which acts like a hidden confounder⁹, or from a much larger measurement error in A than B , which can result in B becoming a better measurement of $A^{(t)}$ than A itself⁸. In this simulation, the false negatives persisted even if $E \rightarrow A$ was observationally much stronger than $E \rightarrow B$, such as when A 's measurement error was only 10% ($\sigma_{A1}^2 = 0.1$) compared to up to 67% for B (Figure 2B). This suggested a unique and mostly neglected source of false negatives that would not affect other tests. Indeed, the secondary, relevance, and controlled tests were much less sensitive to measurement errors (Figure 2A,C,D).

2.5 Findr outperforms traditional causal inference and machine learning methods on microRNA target prediction

In order to evaluate Findr on a real dataset, we performed causal inference on miRNA and mRNA sequencing data in lymphoblastoid cell lines from 360 European individuals in the Geuvadis study³ (Section 4.1). We first tested 55 miRNAs with reported significant cis-eQTLs against 23,722 genes. Since miRNA target predictions from sequence complementarity alone result in high numbers of false positives, prediction methods based on correlating miRNA and gene expression profiles are of great interest²¹. Although miRNA target prediction using causal inference from genotype and gene expression data has been considered²², it remains unknown whether the inclusion of genotype data improves existing expression-based methods. To compare Findr against the state-of-the-art for expression-based miRNA target prediction, we used miRLAB, an integrated database of experimentally confirmed human miRNA target genes with a uniform interface to predict targets using twelve methods, including linear and non-linear, pairwise correlation and multivariate regression methods⁶². We were able to infer miRNA targets with 11/12 miRLAB methods, and also applied the GENIE3 random forest regression method⁶³, CIT, and the three tests in Findr: the new (P) and traditional (P_T) causal inference tests and the correlation test (P_0) (Supplementary Material S2.4). Findr's new test achieved highest AUROC and AUPR among the 16 methods attempted. In particular, Findr's new test significantly outperformed the traditional test and CIT, the two other genotype-assisted methods, while also being over 500,000 times faster than CIT (Figure 3, Table S2, Figure S8). Findr's correlation test outperformed all other methods not using geno-

type information, including correlation, regression, and random forest methods, and was 500 to 100,000 times faster (Figure 3, Table S2, Figure S8). This further illustrates the power of the Bayesian gene-specific background estimation method implemented in all Findr’s tests (Section 4.5).

2.6 Findr predicts transcription factor targets with more accurate FDR estimates

We considered 3,172 genes with significant cis-eQTLs in the Geuvadis data³ (Section 4.1) and inferred regulatory interactions to the 23,722 target genes using Findr’s traditional (P_T), new (P) and correlation (P_0) tests, and CIT. Groundtruths of experimentally confirmed causal gene interactions in human, and mammalian systems more generally, are of limited availability and mainly concern transcription or transcription-associated DNA-binding factors (TFs). Here we focused on a set of 25 TFs in the set of eQTL-genes for which either differential expression data following siRNA silencing (6 TFs) or TF-binding data inferred from ChIP-sequencing and/or DNase footprinting (20 TFs) in a lymphoblastoid cell line (GM12878) was available⁶⁶ (Section 4.1). AUPRs and AUROCs did not exhibit substantial differences, other than modest improvement over random predictions (Figure S9). To test for enrichment of true positives among the top-ranked predictions, which would be missed by global evaluation measures such as AUPR or AUROC, we took advantage of the fact that Findr’s probabilities are empirical local precision estimates for each test (Section 4.5), and assessed how estimated local precisions of new, traditional, and correlation tests reflected the actual precision. Findr’s new test correctly reflected the precision values at various threshold levels, and was able to identify true regulations at high precision control levels (Figure 4). However, the traditional test significantly underestimated precision due to its elevated FNR. This led to a lack of predictions at high precision thresholds but enrichment of true regulations at low thresholds, essentially nullifying the statistical meaning of its output probability P_T . On the other hand, the correlation test significantly overestimated precisions because it is unable to distinguish causal, reversed causal or confounded interactions, which raises its FDR. The same results were observed when alternative groundtruth ChIP-sequencing networks were considered (Figure S9, Figure S10).

3 Discussion

We developed a highly efficient, scalable software package Findr (Fast Inference of Networks from Directed Regulations) implementing novel and existing causal inference tests. Application of Findr on real and simulated genome and transcriptome variation data showed that our novel tests, which account for weak secondary linkage and hidden confounders at the potential cost of an increased number of false positives, resulted in a significantly improved performance to predict known gene regulatory interactions compared to existing methods, particularly traditional methods based on conditional independence tests, which had highly elevated false negative rates.

Causal inference using eQTLs as causal anchors relies on crucial assumptions which have been discussed in-depth elsewhere^{8,9}. Firstly, it is assumed that genetic variation is always causal for variation in gene expression, or quantitative traits more generally, and is independent of any observed or hidden confounding factors. Although this assumption is valid for randomly sampled individuals, caution is required when this is not the case (e.g. case-control studies). Secondly, measurement error is assumed to be independent and comparable across variables. Correlated measurement error acts like a confounding variable, whereas a much larger measurement error in the source variable A than the target variable B may lead to an inversion of the inferred causal direction. The conditional independence test in particular relies on the unrealistic assumptions that hidden confounders and measurement errors are absent, the violation of which incurs false negatives and a failure to correctly predict causal relations, as shown throughout this paper.

Although the newly proposed test avoids the elevated FNR from the conditional independence test, it is not without its own limitations. Unlike the conditional independence test, the relevance and controlled tests (Table 1) are symmetric between the two genes considered. Therefore the direction of causality in the new test arises predominantly from using a different eQTL when testing the reverse interaction, potentially leading to a higher FDR as a minor trade-off. About 10% of cis-regulatory eQTLs are linked (as cis-eQTLs) to the expression of more than one gene²⁶. In these cases, it appears that the shared cis-eQTL regulates the genes independently²⁶, which in Findr is accounted for by the ‘controlled’ test (Table 1). When causality between genes and phenotypes or among phenotypes is tested, sharing or linkage of

(e)QTLs can be more common. Resolving causality in these cases may require the use of Findr’s conservative, traditional causal inference test, in conjunction with the new test.

In this paper we have addressed the challenge of pairwise causal inference, but to reconstruct the actual pathways and networks that affect a phenotypic trait, two important limitations have to be considered. First, linear pathways propagate causality, and may thus appear as densely connected sets of triangles in pairwise causal networks. Secondly, most genes are regulated by multiple upstream factors, and hence some true edges may only have a small posterior probability unless they are considered in an appropriate multivariate context. The most straightforward way to address these issues would be to model the real directed interaction network as a Bayesian network with sparsity constraints. A major advantage of Findr is that it outputs probability values which can be directly incorporated as prior edge probabilities in existing network inference softwares.

In conclusion, Findr is a highly efficient and accurate open source software tool for causal inference from large-scale genome-transcriptome variation data. Its nonparametric nature ensures robust performances across datasets without parameter tuning, with easily interpretable output in the form of accurate precision and FDR estimates. Findr is able to predict causal interactions in the context of complex regulatory networks where unknown upstream regulators confound traditional conditional independence tests, and more generically in any context with discrete or continuous causal anchors.

4 Methods

4.1 Datasets

We used the following datasets/databases for evaluating causal inference methods:

1. Simulated genotype and transcriptome data of synthetic gene regulatory networks from the DREAM5 Systems Genetics challenge A (DREAM for short)⁵⁷, generated by the SysGenSIM software²⁸. DREAM provides 15 sub-datasets, obtained by simulating 100, 300, and 999 samples of 5 different networks each, containing 1000 genes in every sub-dataset but more regulations for sub-datasets with higher numbering. In every sub-dataset, each gene has exactly one matching genotype variable. 25% of the genotype

variables are cis-expression Quantitative Trait Loci (eQTL), defined in DREAM as: their variation changes the expression level of the corresponding gene directly. The other 75% are trans-eQTLs, defined as: their variation affects the expression levels of only the downstream targets of the corresponding gene, but not the gene itself. Because the identities of cis-eQTLs are unknown, we calculated the P-values of genotype-gene expression associations with kruX⁶⁹, and kept all genes with a P-value less than 1/750 to filter out genes without cis-eQTL. For the subsampling analysis (detailed in Section 4.7), we restricted the evaluation to the prediction of target genes from these cis-genes only, in line with the assumption that Findr and other causal inference methods require as input a list of genes whose expression is significantly associated with at least one cis-eQTL. For the full comparison of Findr to the DREAM leaderboard results, we predicted target genes for all genes, regardless of whether they had a cis-eQTL.

2. Genotype and transcriptome sequencing data on 465 human lymphoblastoid cell line samples from the Geuvadis project³ consisting of the following data products:

- Genotype data (ArrayExpress accession E-GEUV-1)³⁰.
- Gene quantification data for 23722 genes from nonredundant unique samples and after quality control and normalization (ArrayExpress accession E-GEUV-1)³¹.
- Quantification data of miRNA, with the same standard as gene quantification data (ArrayExpress accession E-GEUV-2)³².
- Best eQTLs of mRNAs and miRNAs (ArrayExpress accessions E-GEUV-1 and E-GEUV-2)^{33,34}.

We restricted our analysis to 360 European samples which are shared by gene and miRNA quantifications. Excluding invalid eQTLs from the Geuvadis analysis, such as single-valued genotypes, 55 miRNA-eQTL pairs and 3172 gene-eQTL pairs were retained.

3. For validation of predicted miRNA-gene interactions, we extracted the “strong” ground-truth table from miRLAB^{35,62}, which contains experimentally confirmed miRNA-gene regulations from the following databases: TarBase³⁶, miRecords³⁷, miRWalk³⁸, and

miRTarBase³⁹. The intersection of the Geuvadis and ground-truth table contains 20 miRNAs and 1054 genes with 1217 confirmed regulations, which are considered for prediction validation. Interactions that are present in the ground-truth table are regarded as true while others as false.

4. For verification of predicted gene-gene interactions, we obtained differential expression data following siRNA silencing of 59 transcription-associated factors (TFs) and DNA-binding data of 201 TFs for 8872 genes in a reference lymphoblastoid cell line (GM12878) from⁶⁶. Six siRNA-targeted TFs, 20 DNA-binding TFs, and 6,790 target genes without missing differential expression data intersected with the set of 3172 eQTL-genes and 23722 target genes in Geuvadis and were considered for validation. We reproduced the pipeline of⁶⁶ with the criteria for true targets as having a False Discovery Rate (FDR) < 0.05 from R package `qvalue` for differential expression in siRNA silencing, or having at least 2 TF-binding peaks within 10kb of their transcription start site. We also obtained the filtered proximal TF-target network from⁶⁷, which had 14 TFs and 7,000 target genes in common with the Geuvadis data.

4.2 General inference algorithm

Consider a set of observations sampled from a mixture distribution of a null and an alternative hypothesis. For instance in gene regulation, every observation can correspond to expression levels of a pair of genes which are sampled from a bivariate normal distribution with zero (null hypothesis) or non-zero (alternative hypothesis) correlation coefficient. In Findr, we predict the probability that any sample follows the alternative hypothesis with the following algorithm (based on and modified from⁵⁵):

1. For robustness against outliers, we convert every continuous variable into standard normally distributed $N(0, 1)$ values using a rank-based inverse normal transformation across all samples. We name this step as supernormalization.
2. We propose a null and an alternative hypothesis for every likelihood ratio test (LRT) of interest where, by definition, the null hypothesis space is a subset of the alternative hypothesis. Model parameters are replaced with their maximum likelihood estimators

(MLEs) to obtain the log likelihood ratio (LLR) between the alternative and null hypotheses (Section 4.3).

3. We derive the analytical expression for the probability density function (PDF) of the LLR when samples follow the null hypothesis (Section 4.4).
4. We convert LLRs into posterior probabilities of the hypothesis of interest with the empirical estimation of local FDR (Section 4.5).

Implementational details can be found in Findr’s source code.

4.3 Likelihood ratio tests

Consider correlated genes A , B , and a third variable E upstream of A and B , such as a significant eQTL of A . The eQTLs can be obtained either de novo using eQTL identification tools such as matrix-eQTL⁶⁸ or kruX⁶⁹, or from published analyses. Throughout this article, we assume that E is a significant eQTL of A , whereas extension to other data types is straightforward. We use A_i and B_i for the expression levels of gene A and B respectively, which are assumed to have gone through the supernormalization in Section 4.2, and optionally the genotypes of the best eQTL of A as E_i , where $i = 1, \dots, n$ across samples. Genotypes are assumed to have a total of n_a alleles, so $E_i \in \{0, \dots, n_a\}$. We define the null and alternative hypotheses for a total of six tests, as shown in Table 1. LLRs of every test are calculated separately as follows:

0. Correlation test: Define the null hypothesis as A and B are independent, and the alternative hypothesis as they are correlated:

$$\mathcal{H}_{\text{null}}^{(0)} = A \perp B, \quad \mathcal{H}_{\text{alt}}^{(0)} = A \text{ --- } B. \quad (1)$$

The superscript (0) is the numbering of the test. Both hypotheses are modeled with gene expression levels following bivariate normal distributions, as

$$\begin{pmatrix} A_i \\ B_i \end{pmatrix} \sim N \left(\begin{pmatrix} 0 \\ 0 \end{pmatrix}, \begin{pmatrix} \sigma_{A0}^2 & \rho \sigma_{A0} \sigma_{B0} \\ \rho \sigma_{A0} \sigma_{B0} & \sigma_{B0}^2 \end{pmatrix} \right),$$

for $i = 1, \dots, n$. The null hypothesis corresponds to $\rho = 0$.

Maximum likelihood estimators (MLE) for the model parameters ρ , σ_{A0} , and σ_{B0} are

$$\hat{\rho} = \frac{1}{n} \sum_{i=1}^n A_i B_i, \quad \hat{\sigma}_{A0} = \hat{\sigma}_{B0} = 1, \quad (2)$$

and the LLR is simply

$$\text{LLR}^{(0)} = -\frac{n}{2} \ln(1 - \hat{\rho}^2). \quad (3)$$

In the absence of genotype information, we use nonzero correlation between A and B as the indicator for $A \rightarrow B$ regulation, giving the posterior probability

$$P(A \text{ --- } B) = P(\mathcal{H}_{\text{alt}}^{(0)} \mid \text{LLR}^{(0)}).$$

false negative

1. Primary (linkage) test: Verify that E regulates A from $\mathcal{H}_{\text{alt}}^{(1)} \equiv E \rightarrow A$ and $\mathcal{H}_{\text{null}}^{(1)} \equiv E \text{ --- } A$. For $\mathcal{H}_{\text{alt}}^{(1)}$, we model $E \rightarrow A$ as A follows a normal distribution whose mean is determined by E categorically, i.e.

$$A_i \mid E_i \sim N(\mu_{E_i}, \sigma_A^2). \quad (4)$$

From the total likelihood $p(A \mid E) = \prod_{i=1}^n p(A_i \mid E_i)$, we find MLEs for model parameters $\mu_j, j = 0, 1, \dots, n_a$, and σ_A , as

$$\hat{\mu}_j = \frac{1}{n_j} \sum_{i=1}^n A_i \delta_{E_i j}, \quad \hat{\sigma}_A^2 = 1 - \sum_{j=0}^{n_a} \frac{n_j}{n} \hat{\mu}_j^2,$$

where n_j is the sample count by genotype category,

$$n_j \equiv \sum_{i=1}^n \delta_{E_i j}.$$

The Kronecker delta function is defined as $\delta_{xy} = 1$ for $x = y$, and 0 otherwise. When summing over all genotype values ($j = 0, \dots, n_a$), we only pick those that exist ($n_j > 0$) throughout this article. Since the null hypothesis is simply that A_i is sampled from

a genotype-independent normal distribution, with MLEs of mean zero and standard deviation one due to the supernormalization (Section 4.2), the LLR for test 1 becomes

$$\text{LLR}^{(1)} = -\frac{n}{2} \ln \hat{\sigma}_A^2. \quad (5)$$

By favoring a large $\text{LLR}^{(1)}$, we select $\mathcal{H}_{\text{alt}}^{(1)}$ and verify that E regulates A , with

$$P(E \rightarrow A) = P(\mathcal{H}_{\text{alt}}^{(1)} \mid \text{LLR}^{(1)}).$$

2. Secondary (linkage) test: The secondary test is identical with the primary test, except it verifies that E regulates B . Hence repeat the primary test on E and B and obtain the MLEs:

$$\hat{\nu}_j = \frac{1}{n_j} \sum_{i=1}^n B_i \delta_{E_i j}, \quad \hat{\sigma}_B^2 = 1 - \sum_{j=0}^{n_a} \frac{n_j}{n} \hat{\nu}_j^2,$$

and the LLR as

$$\text{LLR}^{(2)} = -\frac{n}{2} \ln \hat{\sigma}_B^2.$$

$\mathcal{H}_{\text{alt}}^{(2)}$ is chosen to verify that E regulates B .

3. (Conditional) independence test: Verify that E and B are independent when conditioning on A . This can be achieved by comparing $\mathcal{H}_{\text{alt}}^{(3)} \equiv B \leftarrow E \rightarrow A \wedge (A \text{ correlates with } B)$ against $\mathcal{H}_{\text{null}}^{(3)} \equiv E \rightarrow A \rightarrow B$. LLRs close to zero then prefer $\mathcal{H}_{\text{null}}^{(3)}$, and ensure that E regulates B only through A :

$$P(E \perp B \mid A) = P(\mathcal{H}_{\text{null}}^{(3)} \mid \text{LLR}^{(3)}).$$

For $\mathcal{H}_{\text{alt}}^{(3)}$, the bivariate normal distribution dependent on E can be represented as

$$\begin{pmatrix} A_i \\ B_i \end{pmatrix} \Bigg| E_i \sim N \left(\begin{pmatrix} \mu_{E_i} \\ \nu_{E_i} \end{pmatrix}, \begin{pmatrix} \sigma_A^2 & \rho \sigma_A \sigma_B \\ \rho \sigma_A \sigma_B & \sigma_B^2 \end{pmatrix} \right).$$

For $\mathcal{H}_{\text{null}}^{(3)}$, the distributions follow Eq 4, as well as

$$B_i \mid A_i \sim N(\rho A_i, \sigma_B^2).$$

Substituting parameters $\mu_j, \nu_j, \sigma_A, \sigma_B, \rho$ of $\mathcal{H}_{\text{alt}}^{(3)}$ and $\mu_j, \rho, \sigma_A, \sigma_B$ of $\mathcal{H}_{\text{null}}^{(3)}$ with their MLEs, we obtain the LLR:

$$\begin{aligned} \text{LLR}^{(3)} &= -\frac{n}{2} \ln (\hat{\sigma}_A^2 \hat{\sigma}_B^2 - (\hat{\rho} + \sigma_{AB} - 1)^2) \\ &\quad + \frac{n}{2} \ln \hat{\sigma}_A^2 + \frac{n}{2} \ln(1 - \hat{\rho}^2), \end{aligned} \quad (6)$$

where

$$\sigma_{AB} \equiv 1 - \sum_{j=0}^{n_a} \frac{n_j}{n} \hat{\mu}_j \hat{\nu}_j,$$

and $\hat{\rho}$ is defined in Eq 2.

4. Relevance test: Since the indirect regulation $E \rightarrow B$ tends to be weaker than any of its direct regulation components ($E \rightarrow A$ or $A \rightarrow B$), we propose to test $E \rightarrow A \rightarrow B$ with indirect regulation $E \rightarrow B$ as well as the direct regulation $A \rightarrow B$ for stronger distinguishing power on weak regulations. We define $\mathcal{H}_{\text{alt}}^{(4)} \equiv E \rightarrow A \wedge E \rightarrow B \leftarrow A$ and $\mathcal{H}_{\text{null}}^{(4)} \equiv E \rightarrow A \quad B$. This simply verifies that B is not independent from both A and E simultaneously. In the alternative hypothesis, B is regulated by E and A , which is modeled as a normal distribution whose mean is additively determined by E categorically and A linearly, i.e.

$$B_i | E_i, A_i \sim N(\nu_{E_i} + \rho A_i, \sigma_B^2).$$

We can hence solve its LLR as

$$\text{LLR}^{(4)} = -\frac{n}{2} \ln (\hat{\sigma}_A^2 \hat{\sigma}_B^2 - (\hat{\rho} + \sigma_{AB} - 1)^2) + \frac{n}{2} \ln \hat{\sigma}_A^2.$$

5. Controlled test: Based on the positives of the secondary test, we can further distinguish the alternative hypothesis $\mathcal{H}_{\text{alt}}^{(5)} \equiv B \leftarrow E \rightarrow A \wedge A \rightarrow B$ from the null $\mathcal{H}_{\text{null}}^{(5)} \equiv B \leftarrow E \rightarrow A$ to verify that E does not regulate A and B independently. Its LLR can be solved as

$$\text{LLR}^{(5)} = -\frac{n}{2} \ln (\hat{\sigma}_A^2 \hat{\sigma}_B^2 - (\hat{\rho} + \sigma_{AB} - 1)^2) + \frac{n}{2} \ln \hat{\sigma}_A^2 \hat{\sigma}_B^2.$$

4.4 Null distributions for the log-likelihood ratios

The null distribution of LLR, $p(\text{LLR} \mid \mathcal{H}_{\text{null}})$, may be obtained either by simulation or analytically. Simulation, such as random permutations from real data or the generation of random data from statistics of real data, can deal with a much broader range of scenarios in which analytical expressions are unattainable. However, the drawbacks are obvious: simulation can take hundreds of times longer than analytical methods to reach a satisfiable precision. Here we obtained analytical expressions of $p(\text{LLR} \mid \mathcal{H}_{\text{null}})$ for all the tests introduced above.

0. Correlation test: $\mathcal{H}_{\text{null}}^{(0)} = A \perp B$ indicates no correlation between A and B . Therefore, we can start from

$$\tilde{B}_i \sim \text{i.i.d } N(0, 1). \quad (7)$$

In order to simulate the supernormalization step, we normalize \tilde{B}_i into B_i with zero mean and unit variance as:

$$B_i \equiv \frac{\tilde{B}_i - \bar{\tilde{B}}}{\sigma_{\tilde{B}}}, \quad \bar{\tilde{B}} \equiv \frac{1}{n} \sum_{i=1}^n \tilde{B}_i, \quad \sigma_{\tilde{B}}^2 \equiv \frac{1}{n} \sum_{i=1}^n (\tilde{B}_i - \bar{\tilde{B}})^2. \quad (8)$$

Transform the random variables $\{\tilde{B}_i\}$ by defining

$$X_1 \equiv \frac{1}{\sqrt{n}} \sum_{i=1}^n A_i \tilde{B}_i, \quad (9)$$

$$X_2 \equiv \frac{1}{\sqrt{n}} \sum_{i=1}^n \tilde{B}_i, \quad (10)$$

$$X_3 \equiv \left(\sum_{i=1}^n \tilde{B}_i^2 \right) - X_1^2 - X_2^2. \quad (11)$$

Since $\tilde{B}_i \sim \text{i.i.d } N(0, 1)$ (according to Eq 7), we can easily verify that X_1, X_2, X_3 are independent, and

$$X_1 \sim N(0, 1), \quad X_2 \sim N(0, 1), \quad X_3 \sim \chi^2(n-2). \quad (12)$$

Expressing Eq 3 in terms of X_1, X_2, X_3 gives

$$\text{LLR}^{(0)} = -\frac{n}{2} \ln(1 - Y), \quad (13)$$

in which

$$Y \equiv \frac{X_1^2}{X_1^2 + X_3} \sim \text{Beta}\left(\frac{1}{2}, \frac{n-2}{2}\right) \quad (14)$$

follows the Beta distribution.

We define distribution $\mathcal{D}(k_1, k_2)$ as the distribution of a random variable $Z = -\frac{1}{2} \ln(1 - Y)$ for $Y \sim \text{Beta}(k_1/2, k_2/2)$, i.e.

$$Z = -\frac{1}{2} \ln(1 - Y) \sim \mathcal{D}(k_1, k_2).$$

The probability density function (PDF) for $Z \sim \mathcal{D}(k_1, k_2)$ can be derived as: for $z > 0$,

$$p(z | k_1, k_2) = \frac{2}{B(k_1/2, k_2/2)} (1 - e^{-2z})^{(k_1/2-1)} e^{-k_2z}, \quad (15)$$

and for $z \leq 0$, $p(z | k_1, k_2) = 0$. Here $B(a, b)$ is the Beta function. Therefore the null distribution for the correlation test is simply

$$\text{LLR}^{(0)}/n \sim \mathcal{D}(1, n-2). \quad (16)$$

1. Primary test: $\mathcal{H}_{\text{null}}^{(1)} = E$ A indicates no regulation from E to A . Therefore, similarly with the correlation test, we start from $\tilde{A}_i \sim \text{i.i.d } N(0, 1)$ and normalize them to A_i with zero mean and unit variance.

The expression of $\text{LLR}^{(1)}$ then becomes:

$$\text{LLR}^{(1)} = -\frac{n}{2} \ln \left(1 - \sum_{j=0}^{n_a} \frac{n_j}{n} \frac{(\hat{\mu}_j - \bar{A})^2}{\sigma_A^2} \right),$$

where

$$\hat{\mu}_j \equiv \frac{1}{n_j} \sum_{i=1}^n \tilde{A}_i \delta_{E_i j}.$$

For now, assume all possible genotypes are present, i.e. $n_j > 0$ for $j = 0, \dots, n_a$. Trans-

form $\{\tilde{A}_i\}$ by defining

$$\begin{aligned} X_j &\equiv \sqrt{n_j} \hat{\mu}_j, & \text{for } j = 0, \dots, n_a, \\ X_{n_a+1} &\equiv \left(\sum_{i=1}^n \tilde{A}_i^2 \right) - \left(\sum_{j=0}^{n_a} X_j^2 \right). \end{aligned} \quad (17)$$

Then we can similarly verify that $\{X_i\}$ are pairwise independent, and

$$\begin{aligned} X_i &\sim N(0, 1), \text{ for } i = 0, \dots, n_a, \\ X_{n_a+1} &\sim \chi^2(n - n_a - 1). \end{aligned} \quad (18)$$

Again transform $\{X_i\}$ by defining independent random variables

$$\begin{aligned} Y_1 &\equiv \sum_{j=0}^{n_a} \sqrt{\frac{n_j}{n}} X_j \sim N(0, 1), \\ Y_2 &\equiv \left(\sum_{j=0}^{n_a} X_j^2 \right) - Y_1^2 \sim \chi^2(n_a), \\ Y_3 &\equiv X_{n_a+1} \sim \chi^2(n - n_a - 1). \end{aligned}$$

Some calculation would reveal

$$\text{LLR}^{(1)} = -\frac{n}{2} \ln \left(1 - \frac{Y_2}{Y_2 + Y_3} \right),$$

i.e.

$$\text{LLR}^{(1)}/n \sim \mathcal{D}(n_a, n - n_a - 1).$$

To account for genotypes that do not show up in the samples, define $n_v \equiv \sum_{j \in \{j|n_j > 0\}} 1$ as the number of different genotype values across all samples. Then

$$\text{LLR}^{(1)}/n \sim \mathcal{D}(n_v - 1, n - n_v). \quad (19)$$

2. Secondary test: Since the null hypotheses and LLRs of primary and secondary tests are identical, $\text{LLR}^{(2)}$ follows the same null distribution as Eq 19.

3. Independence test: The independence test verifies if E and B are uncorrelated when conditioning on A , with $\mathcal{H}_{\text{null}}^{(3)} = E \rightarrow A \rightarrow B$. For this purpose, we keep E and A intact while randomizing \tilde{B}_i according to B 's correlation with A :

$$\tilde{B}_i \equiv \hat{\rho}A_i + \sqrt{1 - \hat{\rho}^2} X_i, \quad X_i \sim \text{i.i.d } N(0, 1).$$

Then \tilde{B}_i is normalized to B_i according to Eq 8. The null distribution of $\text{LLR}^{(3)}$ can be obtained with similar but more complex computations from Eq 6, as

$$\text{LLR}^{(3)}/n \sim \mathcal{D}(n_v - 1, n - n_v - 1). \quad (20)$$

4. Relevance test: The null distribution of $\text{LLR}^{(4)}$ can be obtained similarly by randomizing B_i according to Eq 7 and Eq 8, as

$$\text{LLR}^{(4)}/n \sim \mathcal{D}(n_v, n - n_v - 1).$$

5. Controlled test: To compute the null distribution for the controlled test, we start from

$$\tilde{B}_i = \hat{\nu}_{E_i} + \hat{\sigma}_B X_i, \quad X_i \sim N(0, 1), \quad (21)$$

and then normalize \tilde{B}_i into B_i according to Eq 8. Some calculation reveals the null distribution as

$$\text{LLR}^{(5)}/n \sim \mathcal{D}(1, n - n_v - 1).$$

We verified our analytical method of deriving null distributions by comparing the analytical null distribution v.s. null distribution from permutation for the relevance test in Section S2.2.

4.5 Bayesian inference of posterior probabilities

After obtaining the PDFs for the LLRs from real data and the null hypotheses, we can convert LLR values into posterior probabilities $P(\mathcal{H}_{\text{alt}} | \text{LLR})$. We use a similar technique as in⁵⁵, which itself was based on a more general framework to estimate local FDRs in genome-wide studies⁴². This framework assumes that the real distribution of a certain test statistic forms

a mixture distribution of null and alternative hypotheses. After estimating the null distribution, either analytically or by simulation, it can be compared against the real distribution to determine the proportion of null hypotheses, and consequently the posterior probability that the alternative hypothesis is true at any value of the statistic.

To be precise, consider an arbitrary likelihood ratio test. The fundamental assumption is that in the limit $\text{LLR} \rightarrow 0^+$, all test cases come from the null hypothesis ($\mathcal{H}_{\text{null}}$), whilst as LLR increases, the proportion of alternative hypotheses (\mathcal{H}_{alt}) also grows. The mixture distribution of real LLR values is assumed to have a PDF as

$$p(\text{LLR}) = P(\mathcal{H}_{\text{null}})p(\text{LLR} | \mathcal{H}_{\text{null}}) + P(\mathcal{H}_{\text{alt}})p(\text{LLR} | \mathcal{H}_{\text{alt}}).$$

The priors $P(\mathcal{H}_{\text{null}})$ and $P(\mathcal{H}_{\text{alt}})$ sum to unity and correspond to the proportions of null and alternative hypotheses in the mixture distribution. For any test $i = 0, \dots, 5$, Bayes' theorem then yields its posterior probability as

$$P(\mathcal{H}_{\text{alt}}^{(i)} | \text{LLR}^{(i)}) = \frac{p(\text{LLR}^{(i)} | \mathcal{H}_{\text{alt}}^{(i)})}{p(\text{LLR}^{(i)})} P(\mathcal{H}_{\text{alt}}^{(i)}). \quad (22)$$

Based on this, we can define the posterior probabilities of the selected hypotheses according to Table 1, i.e. the alternative for tests 0, 1, 2, 4, 5 and the null for test 3 as

$$P_i \equiv \begin{cases} P(\mathcal{H}_{\text{alt}}^{(i)} | \text{LLR}^{(i)}), & i = 0, 1, 2, 4, 5, \\ P(\mathcal{H}_{\text{null}}^{(i)} | \text{LLR}^{(i)}), & i = 3. \end{cases} \quad (23)$$

After obtaining the LLR distribution of the null hypothesis [$p(\text{LLR} | \mathcal{H}_{\text{null}})$], we can determine its proportion [$P(\mathcal{H}_{\text{null}})$] by aligning $p(\text{LLR} | \mathcal{H}_{\text{null}})$ with the real distribution $p(\text{LLR})$ at the $\text{LLR} \rightarrow 0^+$ side. This provides all the prerequisites to perform Bayesian inference and obtain any P_i from Eq 23.

In practice, PDFs are approximated with histograms. This requires proper choices of histogram bin widths, $P(\mathcal{H}_{\text{null}})$, and techniques to ensure the conversion from LLR to posterior probability is monotonically increasing and smooth. Implementational details can be found in Findr package and in Section S1.1. Distributions can be estimated either separately for every (E, A) pair or by pooling across all (E, A) pairs. In practice, we test on the order of 10^3 to

10^4 candidate targets (“ B ”) for every (E, A) such that a separate conversion of LLR values to posterior probabilities is both feasible and recommended, as it accounts for different roles of every gene, especially hub genes, through different rates of alternative hypotheses.

Lastly, in a typical application of Findr, inputs of (E, A) pairs will have been pre-determined as the set of significant eQTL-gene pairs from a genome-wide eQTL association analysis. In such cases, we may naturally assume $P_1 = 1$ for all considered pairs, and skip the primary test.

4.6 Tests to evaluate

Based on the six tests in Section 4.3, we use the following tests and test combinations for the inference of genetic regulations, and evaluate them in the results.

- The correlation test is introduced as a benchmark, against which we can compare other methods involving genotype information. Pairwise correlation is a simple measure for the probability of two genes being functionally related either through direct or indirect regulation, or through coregulation by a third factor. Bayesian inference additionally considers different gene roles. Its predicted posterior probability for regulation is P_0 .
- The traditional causal inference test, as explained in⁵⁵, suggested that the regulatory relation $E \rightarrow A \rightarrow B$ can be confirmed with the combination of three separate tests: E regulates A , E regulates B , and E only regulates B through A (i.e. E and B become independent when conditioning on A). They correspond to the primary, secondary, and independence tests respectively. The regulatory relation $E \rightarrow A \rightarrow B$ is regarded positive only when all three tests return positive. The three tests filter the initial hypothesis space of all possible relations between E , A , and B , sequentially to $E \rightarrow A$ (primary test), $E \rightarrow A \wedge E \rightarrow B$ (secondary test), and $E \rightarrow A \rightarrow B \wedge$ (no confounder for A and B) (conditional independence test). The resulting test is stronger than $E \rightarrow A \rightarrow B$ by disallowing confounders for A and B . So its probability can be broken down as

$$P_T \equiv P_1 P_2 P_3. \tag{24}$$

Trigger⁴³ is an R package implementation of the method. However, since Trigger in-

tegrates eQTL discovery with causal inference, it is not practical for use on modern datasets. For this reason, we reimplemented this method in Findr, and evaluated it with P_2 and P_2P_3 separately, in order to assess the individual effects of secondary and independence tests. As discussed above, we expect a set of significant eQTLs and their associated genes as input, and therefore $P_1 = 1$ is assured and not calculated in this paper or the package Findr. Note that P_T is the estimated local precision, i.e. the probability that tests 2 and 3 are both true. Correspondingly, its local FDR (the probability that one of them is false) is $1 - P_T$.

- The novel test, aimed specifically at addressing the failures of the traditional causal inference test, combines the tests differently:

$$P \equiv \frac{1}{2}(P_2P_5 + P_4). \quad (25)$$

Specifically, the first term in Eq 25 accounts for hidden confounders. The controlled test replaces the conditional independence test and constrains the hypothesis space more weakly, only requiring the correlation between A and B is not entirely due to pleiotropy. Therefore, P_2P_5 (with $P_1 = 1$) verifies the hypothesis that $B \leftarrow E \rightarrow A \wedge (A \not\perp B \mid E)$, a superset of $E \rightarrow A \rightarrow B$.

On the other hand, the relevance test in the second term of Eq 25 addresses weak interactions that are undetectable by the secondary test from existing data (P_2 close to 0). This term still grants higher-than-null significance to weak interactions, and verifies that $E \rightarrow A \wedge (E \rightarrow B \vee A \text{ --- } B)$, also a superset of $E \rightarrow A \rightarrow B$. In the extreme undetectable limit where $P_2 = 0$ but $P_4 \neq 0$, the novel test Eq 25 automatically reduces to $P = \frac{1}{2}P_4$, which assumes equal probability of either direction and assigns half of the relevance test probability to $A \rightarrow B$.

The composite design of the novel test aims not to miss any genuine regulation whilst distinguishing the full spectrum of possible interactions. When the signal level is too weak for tests 2 and 5, we expect P_4 to still provide distinguishing power better than random predictions. When the interaction is strong, P_2P_5 is then able to pick up true targets regardless of the existence of hidden confounders.

4.7 Evaluation methods

- Evaluation metrics:

Given the predicted posterior probabilities for every pair (A, B) from any test, or more generically a score from any inference method, we evaluated the predictions against the direct regulations in the ground-truth tables (Section 4.1) with the metrics of Receiver Operating Characteristic (ROC) and Precision-Recall (PR) curves, as well as the Areas Under the ROC (AUROC) and Precision-Recall (AUPR) curves⁴⁴. In particular, AUPR is calculated with the Davis-Goadrich nonlinear interpolation⁴⁵ with R package PRROC.

- Subsampling:

In order to assess the effect of sample size on the performances of inference methods, we performed subsampling evaluations. This is made practically possible by the DREAM datasets which contain 999 samples with sufficient variance, as well as the computational efficiency from Findr which makes subsampling computationally feasible. With a given dataset and ground-truth table, the total number of samples n , and the number of samples of our actual interest $N < n$, we performed subsampling by repeating following steps k times:

1. Randomly select N samples out of the total n samples without replacement.
2. Infer regulations only based on the selected samples.
3. Compute and record the evaluation metrics of interest (e.g. AUROC and AUPR) with the inference results and ground-truths.

Evaluation metrics are recorded in every loop, and their means, standard deviations, and standard errors over the k runs, are calculated. The mean indicates how the inference method performs on the metric in average, while the standard deviation reflects how every individual subsampling deviates from the average performance.

- Local precision of top predictions separately for confounded and unconfounded gene pairs:

In order to demonstrate the inferential precision among top predictions for any inference test (here the traditional and novel tests separately), we first ranked all (ordered) gene

pairs (A, B) according to the inferred significance for $A \rightarrow B$. All gene pairs were split into groups according to their relative significance ranking (9 groups in Figure 1C,D, as top 0% to 0.01%, 0.01% to 0.02%, etc). Each group was divided into two subgroups, based on whether each gene pair shared at least one direct upstream regulator gene (confounded) or not (unconfounded), according to the gold standard. Within each subgroup, the local precision was computed as the number of true directed regulations divided by the total number of gene pairs in the subgroup.

4.8 Simulation studies on causal models with measurement error

We investigated how each statistical test tolerates measurement errors with simulations in a controlled setting. We modelled the causal relation $A \rightarrow B$ in a realistic setup as $E \rightarrow A^{(t)} \rightarrow B$ with $A^{(t)} \rightarrow A$. E remains as the accurately measured genotype values as the eQTL for the primary target gene A . $A^{(t)}$ is the true expression level of gene A , which is not observable. A is the measured expression level for gene A , containing measurement errors. B is the measured expression level for gene B .

For simplicity, we only considered monoallelic species. Therefore the genotype E in each sample followed the Bernoulli distribution, parameterized by the predetermined minor allele frequency. Each regulatory relation (of $E \rightarrow A^{(t)}$, $A^{(t)} \rightarrow A$, and $A^{(t)} \rightarrow B$) corresponded to a normal distribution whose mean was linearly dependent on the regulator variable. In particular, for sample i :

$$A_i^{(t)} \sim N(\widetilde{E}_i, \sigma_{A1}^2), \quad (26)$$

$$A_i \sim N(A_i^{(t)}, \sigma_{A2}^2), \quad (27)$$

$$B_i \sim N(\widetilde{A}_i^{(t)}, \sigma_B^2), \quad (28)$$

in which σ_{A1} , σ_{A2} , and σ_B are parameters of the model. Note that σ_B^2 is B 's variance from all unknown sources, including expression level variations and measurement errors. The tilde normalizes the variable into zero mean and unit variance, as:

$$\widetilde{X}_i \equiv \frac{X_i - \bar{X}}{\sqrt{\text{Var}(X)}}, \quad (29)$$

where \bar{X} and $\text{Var}(X)$ are the mean and variance of $X \equiv \{X_i\}$ respectively.

Given the five parameters of the model (the number of samples, the minor allele frequency, σ_{A1} , σ_{A2} , and σ_B), we could simulate the observed data for E , A , and B , which were then fed into Findr for tests 2-5 and their p-values of the respective null hypotheses. Supernormalization step was replaced with normalization which merely shifted and scaled variables into zero mean and unit variance.

We then chose different configurations on the number of samples, the minor allele frequency, and σ_B . For each configuration, we varied σ_{A1} and σ_{A2} in a wide range to obtain a 2-dimensional heatmap plot for the p-value of each test, thereby exploring how each test was affected by measurement errors of different strengths. Only tiles with a significant $E \rightarrow A$ eQTL relation were retained. The same initial random seed was employed for different configurations to allow for replicability.

Acknowledgements

This work was supported by the BBSRC (grant numbers BB/J004235/1 and BB/M020053/1).

References

1. Albert FW, Kruglyak L. The role of regulatory variation in complex traits and disease. *Nature Reviews Genetics*. 2015;16:197–212.
2. Civelek M, Lusis AJ. Systems genetics approaches to understand complex traits. *Nature Reviews Genetics*. 2014;15(1):34–48.
3. Lappalainen T, Sammeth M, Friedlander MR, /t Hoen PAC, Monlong J, Rivas MA, et al. Transcriptome and genome sequencing uncovers functional variation in humans. *Nature*. 2013 09;501(7468):506–511. Available from: <http://dx.doi.org/10.1038/nature12531>.
4. Ardlie KG, Deluca DS, Segrè AV, Sullivan TJ, Young TR, Gelfand ET, et al. The Genotype-Tissue Expression (GTEx) pilot analysis: Multitissue gene regulation in humans. *Science*. 2015;348(6235):648–660.

5. Franzén O, Ermel R, Cohain A, Akers N, Di Narzo A, Talukdar H, et al. Cardiometabolic Risk Loci Share Downstream Cis and Trans Genes Across Tissues and Diseases. *Science*. 2016;.
6. Schadt EE. Molecular networks as sensors and drivers of common human diseases. *Nature*. 2009;461:218–223.
7. Talukdar H, Foroughi Asl H, Jain R, Ermel R, Ruusalepp A, Franzén O, et al. Cross-tissue regulatory gene networks in coronary artery disease. *Cell Systems*. 2016;2:196–208.
8. Rockman MV. Reverse engineering the genotype–phenotype map with natural genetic variation. *Nature*. 2008;456(7223):738–744.
9. Li Y, Tesson BM, Churchill GA, Jansen RC. Critical reasoning on causal inference in genome-wide linkage and association studies. *Trends in Genetics*. 2010;26(12):493–498.
10. Schadt EE, Lamb J, Yang X, Zhu J, Edwards S, GuhaThakurta D, et al. An integrative genomics approach to infer causal associations between gene expression and disease. *Nature Genetics*. 2005;37(7):710–717.
11. Chen L, Emmert-Streib F, Storey J. Harnessing naturally randomized transcription to infer regulatory relationships among genes. *Genome Biology*. 2007;8(10):R219. Available from: <http://genomebiology.com/2007/8/10/R219>.
12. Aten JE, Fuller TF, Lusk AJ, Horvath S. Using genetic markers to orient the edges in quantitative trait networks: the NEO software. *BMC Systems Biology*. 2008;2(1):34.
13. Millstein J, Zhang B, Zhu J, Schadt EE. Disentangling molecular relationships with a causal inference test. *BMC Genetics*. 2009;10(1):1–15. Available from: <http://dx.doi.org/10.1186/1471-2156-10-23>.
14. Neto EC, Broman AT, Keller MP, Attie AD, Zhang B, Zhu J, et al. Modeling causality for pairs of phenotypes in system genetics. *Genetics*. 2013;193(3):1003–1013.
15. Millstein J, Chen GK, Breton CV. cit: hypothesis testing software for mediation analysis in genomic applications. *Bioinformatics*. 2016;32(15):2364–2365. Available from: <http://bioinformatics.oxfordjournals.org/content/32/15/2364.abstract>.
16. Gitter A, Siegfried Z, Klutstein M, Fornes O, Oliva B, Simon I, et al. Backup in gene regulatory networks explains differences between binding and knockout results. *Mol Syst Biol*. 2009;5(1).
17. Alon U. Network motifs: theory and experimental approaches. *Nat Rev Genet*.

- 2007;8:450–461.
18. Ritchie ME, Phipson B, Wu D, Hu Y, Law CW, Shi W, et al. limma powers differential expression analyses for RNA-sequencing and microarray studies. *Nucleic Acids Research*. 2015;43(7):e47.
 19. Cole SR, Platt RW, Schisterman EF, Chu H, Westreich D, Richardson D, et al. Illustrating bias due to conditioning on a collider. *International Journal of Epidemiology*. 2010;39(2):417. Available from: [+http://dx.doi.org/10.1093/ije/dyp334](http://dx.doi.org/10.1093/ije/dyp334).
 20. Greenland S. The effect of misclassification in the presence of covariates. *American Journal of Epidemiology*. 1980 Oct;112(4):564–569. Available from: <https://academic.oup.com/aje/article/112/4/564/59323/THE-EFFECT-OF-MISCLASSIFICATION-IN-THE-PRESENCE-OF>.
 21. Huang JC, Babak T, Corson TW, Chua G, Khan S, Gallie BL, et al. Using expression profiling data to identify human microRNA targets. *Nat Meth*. 2007 12;4(12):1045–1049. Available from: <http://dx.doi.org/10.1038/nmeth1130>.
 22. Su WL, Kleinhanz RR, Schadt EE. Characterizing the role of miRNAs within gene regulatory networks using integrative genomics techniques. *Molecular Systems Biology*. 2011;7(1). Available from: <http://msb.embopress.org/content/7/1/490>.
 23. Le TD, Zhang J, Liu L, Liu H, Li J. miRLAB: An R Based Dry Lab for Exploring miRNA-mRNA Regulatory Relationships. *PLoS ONE*. 2015 12;10(12):1–15. Available from: <http://dx.doi.org/10.1371/journal.pone.0145386>.
 24. Huynh-Thu VA, Irrthum A, Wehenkel L, Geurts P. Inferring Regulatory Networks from Expression Data Using Tree-Based Methods. *PLoS ONE*. 2010 09;5(9):1–10. Available from: <http://dx.doi.org/10.1371/journal.pone.0012776>.
 25. Cusanovich DA, Pavlovic B, Pritchard JK, Gilad Y. The functional consequences of variation in transcription factor binding. *PLoS Genetics*. 2014;10(3):e1004226.
 26. Tong P, Monahan J, Prendergast JG. Shared regulatory sites are abundant in the human genome and shed light on genome evolution and disease pleiotropy. *PLoS genetics*. 2017;13(3):e1006673.
 27. DREAM5 Systems Genetics challenges [webpage]; 2014. Available from: <https://www.synapse.org/#!/Synapse:syn2820440/wiki/>.
 28. Pinna A, Soranzo N, Hoeschele I, de la Fuente A. Simulating systems genetics data

- with SysGenSIM. *Bioinformatics*. 2011;27(17):2459–2462. Available from: <http://bioinformatics.oxfordjournals.org/content/27/17/2459.abstract>.
29. Qi J, Foroughi Asl H, Bjorkegren J, Michoel T. kruX: matrix-based non-parametric eQTL discovery. *BMC Bioinformatics*. 2014;15(1):11. Available from: <http://www.biomedcentral.com/1471-2105/15/11>.
 30. Geuvaris genotype data [database on the Internet]. 2013. Available from: <ftp://ftp.ebi.ac.uk/pub/databases/microarray/data/experiment/GEUV/E-GEUV-1/genotypes/>.
 31. Geuvaris gene expression data [database on the Internet]. 2013. Available from: ftp://ftp.ebi.ac.uk/pub/databases/microarray/data/experiment/GEUV/E-GEUV-1/analysis_results/GD462.GeneQuantRPKM.50FN.samplename.resk10.txt.gz.
 32. Geuvaris miRNA expression data [database on the Internet]. 2013. Available from: ftp://ftp.ebi.ac.uk/pub/databases/microarray/data/experiment/GEUV/E-GEUV-2/analysis_results/GD452.MirnaQuantCount.1.2N.50FN.samplename.resk10.txt.
 33. Geuvaris best eQTL data for mRNA [database on the Internet]. 2013. Available from: ftp://ftp.ebi.ac.uk/pub/databases/microarray/data/experiment/GEUV/E-GEUV-1/analysis_results/EUR373.gene.cis.FDR5.best.rs137.txt.gz.
 34. Geuvaris best eQTL data for miRNA [database on the Internet]. 2013. Available from: ftp://ftp.ebi.ac.uk/pub/databases/microarray/data/experiment/GEUV/E-GEUV-2/analysis_results/EUR363.mi.cis.FDR5.best.rs137.txt.gz.
 35. miRLAB ‘strong’ ground-truth data [database on the Internet]. 2015. Available from: https://downloads.sourceforge.net/project/mirlab/groundtruth_Strong.csv.
 36. Vergoulis T, Vlachos IS, Alexiou P, Georgakilas G, Maragkakis M, Reczko M, et al. TarBase 6.0: capturing the exponential growth of miRNA targets with experimental support. *Nucleic Acids Research*. 2012;40(D1):D222–D229. Available from: <http://nar.oxfordjournals.org/content/40/D1/D222.abstract>.
 37. Xiao F, Zuo Z, Cai G, Kang S, Gao X, Li T. miRecords: an integrated resource for microRNA–target interactions. *Nucleic Acids Research*. 2009;37(suppl 1):D105–D110. Available from: http://nar.oxfordjournals.org/content/37/suppl_1/D105.abstract.
 38. Dweep H, Sticht C, Pandey P, Gretz N. miRWalk - Database: Prediction of possible

- miRNA binding sites by “walking” the genes of three genomes. *Journal of Biomedical Informatics*. 2011;44(5):839–847. Available from: <http://dx.doi.org/10.1016/j.jbi.2011.05.002>.
39. Hsu SD, Tseng YT, Shrestha S, Lin YL, Khaleel A, Chou CH, et al. miRTarBase update 2014: an information resource for experimentally validated miRNA-target interactions. *Nucleic Acids Research*. 2014;42(D1):D78–D85. Available from: <http://nar.oxfordjournals.org/content/42/D1/D78.abstract>.
 40. Gerstein MB, Kundaje A, Hariharan M, Landt SG, Yan KK, Cheng C, et al. Architecture of the human regulatory network derived from ENCODE data. *Nature*. 2012;489(7414):91–100.
 41. Shabalin AA. Matrix eQTL: ultra fast eQTL analysis via large matrix operations. *Bioinformatics*. 2012;28(10):1353–1358. Available from: <http://bioinformatics.oxfordjournals.org/content/28/10/1353.abstract>.
 42. Storey JD, Tibshirani R. Statistical significance for genomewide studies. *Proceedings of the National Academy of Sciences*. 2003;100(16):9440–9445. Available from: <http://www.pnas.org/content/100/16/9440.abstract>.
 43. Chen LS, Sangurdekar DP, Storey JD. trigger: Transcriptional Regulatory Inference from Genetics of Gene Expression; 2007. R package version 1.16.0.
 44. Stolovitzky G, Prill RJ, Califano A. Lessons from the DREAM2 Challenges. *Annals of the New York Academy of Sciences*. 2009;1158(1):159–195.
 45. Davis J, Goadrich M. The Relationship Between Precision-Recall and ROC Curves. In: *Proceedings of the 23rd International Conference on Machine Learning. ICML '06*. New York, NY, USA: ACM; 2006. p. 233–240. Available from: <http://doi.acm.org/10.1145/1143844.1143874>.
 46. Wasserman L. *All of statistics: a concise course in statistical inference*. Springer Science & Business Media; 2013.
 47. Vignes M, Vandiel J, Allouche D, Ramadan-Alban N, Cierco-Ayrolles C, Schiex T, et al. Gene regulatory network reconstruction using Bayesian networks, the Dantzig Selector, the Lasso and their meta-analysis. *PloS one*. 2011;6(12):e29165.
 48. Ackermann M, Clément-Ziza M, Michaelson JJ, Beyer A. Teamwork: improved eQTL mapping using combinations of machine learning methods. *PloS one*. 2012;7(7):e40916.

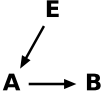
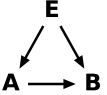
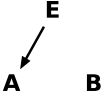
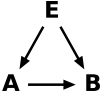
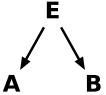
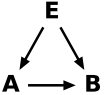
49. Flassig RJ, Heise S, Sundmacher K, Klamt S. An effective framework for reconstructing gene regulatory networks from genetical genomics data. *Bioinformatics*. 2013;29(2):246–254.
50. Huynh-Thu VA, Wehenkel L, Geurts P. Gene Regulatory Network Inference from Systems Genetics Data Using Tree-Based Methods. *Gene Network Inference: Verification of Methods for Systems Genetics Data*. 2014;p. 63.
51. Aten J, Fuller T, Lusi A, Horvath S. Using genetic markers to orient the edges in quantitative trait networks: The NEO software. *BMC Systems Biology*. 2008;2(1):34. Available from: <http://www.biomedcentral.com/1752-0509/2/34>.
52. Liu B, de la Fuente A, Hoeschele I. Gene Network Inference via Structural Equation Modeling in Genetical Genomics Experiments. *Genetics*. 2008;178(3):1763–1776. Available from: <http://www.genetics.org/content/178/3/1763>.
53. Zhu J, Zhang B, Smith EN, Drees B, Brem RB, Kruglyak L, et al. Integrating large-scale functional genomic data to dissect the complexity of yeast regulatory networks. *Nat Genet*. 2008 07;40(7):854–861. Available from: <http://dx.doi.org/10.1038/ng.167>.
54. Chaibub Neto E, Keller MP, Attie AD, Yandell BS. Causal graphical models in systems genetics: A unified framework for joint inference of causal network and genetic architecture for correlated phenotypes. *Ann Appl Stat*. 2010 03;4(1):320–339. Available from: <http://dx.doi.org/10.1214/09-A0AS288>.
55. Lin Chen, Frank Emmert-Streib, and John Storey. Harnessing naturally randomized transcription to infer regulatory relationships among genes. *Genome Biology*, 8(10):R219, 2007.
56. Larry Wasserman. *All of statistics: a concise course in statistical inference*. Springer Science & Business Media, 2013.
57. DREAM5 Systems Genetics challenges, 2014.
58. Matthieu Vignes, Jimmy Vandell, David Allouche, Nidal Ramadan-Alban, Christine Cierco-Ayrolles, Thomas Schiex, Brigitte Mangin, and Simon De Givry. Gene regulatory network reconstruction using bayesian networks, the dantzig selector, the Lasso and their meta-analysis. *PloS one*, 6(12):e29165, 2011.
59. Marit Ackermann, Mathieu Clément-Ziza, Jacob J Michaelson, and Andreas Beyer. Teamwork: improved eQTL mapping using combinations of machine learning methods.

PloS one, 7(7):e40916, 2012.

60. Robert J Flassig, Sandra Heise, Kai Sundmacher, and Steffen Klamt. An effective framework for reconstructing gene regulatory networks from genetical genomics data. *Bioinformatics*, 29(2):246–254, 2013.
61. Vân Anh Huynh-Thu, Louis Wehenkel, and Pierre Geurts. Gene regulatory network inference from systems genetics data using tree-based methods. *Gene Network Inference: Verification of Methods for Systems Genetics Data*, page 63, 2014.
62. Thuc Duy Le, Junpeng Zhang, Lin Liu, Huawen Liu, and Jiuyong Li. mirlab: An r based dry lab for exploring mirna-mrna regulatory relationships. *PLoS ONE*, 10(12):1–15, 12 2015.
63. Vân Anh Huynh-Thu, Alexandre Irrthum, Louis Wehenkel, and Pierre Geurts. Inferring regulatory networks from expression data using tree-based methods. *PLoS ONE*, 5(9):1–10, 09 2010.
64. Joshua Millstein, Bin Zhang, Jun Zhu, and Eric E. Schadt. Disentangling molecular relationships with a causal inference test. *BMC Genetics*, 10(1):1–15, 2009.
65. Joshua Millstein, Gary K. Chen, and Carrie V. Breton. cit: hypothesis testing software for mediation analysis in genomic applications. *Bioinformatics*, 32(15):2364–2365, 2016.
66. Darren A Cusanovich, Bryan Pavlovic, Jonathan K Pritchard, and Yoav Gilad. The functional consequences of variation in transcription factor binding. *PLoS Genetics*, 10(3):e1004226, 2014.
67. M.B. Gerstein, A. Kundaje, M. Hariharan, S.G. Landt, K.K. Yan, C. Cheng, X.J. Mu, E. Khurana, J. Rozowsky, R. Alexander, et al. Architecture of the human regulatory network derived from ENCODE data. *Nature*, 489(7414):91–100, 2012.
68. Andrey A. Shabalin. Matrix eqtl: ultra fast eqtl analysis via large matrix operations. *Bioinformatics*, 28(10):1353–1358, 2012.
69. Jianlong Qi, Hassan Foroughi Asl, Johan Bjorkegren, and Tom Michoel. krux: matrix-based non-parametric eqtl discovery. *BMC Bioinformatics*, 15(1):11, 2014.
70. Jason Aten, Tova Fuller, Aldons Lusi, and Steve Horvath. Using genetic markers to orient the edges in quantitative trait networks: The neo software. *BMC Systems Biology*, 2(1):34, 2008.
71. Bing Liu, Alberto de la Fuente, and Ina Hoeschele. Gene network inference via structural

- equation modeling in genetical genomics experiments. *Genetics*, 178(3):1763–1776, 2008.
72. Jun Zhu, Bin Zhang, Erin N Smith, Becky Drees, Rachel B Brem, Leonid Kruglyak, Roger E Bumgarner, and Eric E Schadt. Integrating large-scale functional genomic data to dissect the complexity of yeast regulatory networks. *Nat Genet*, 40(7):854–861, 07 2008.
73. Elias Chaibub Neto, Mark P. Keller, Alan D. Attie, and Brian S. Yandell. Causal graphical models in systems genetics: A unified framework for joint inference of causal network and genetic architecture for correlated phenotypes. *Ann. Appl. Stat.*, 4(1):320–339, 03 2010.

Table 1: Six likelihood ratio tests are performed to test the regulation $A \rightarrow B$, numbered, named, and defined as shown. E is the best eQTL of A . Arrows in a hypothesis indicate directed regulatory relations. Genes A and B each follow a normal distribution, whose mean depends additively on its regulator(s), as determined in the corresponding hypothesis. The dependency is categorical on discrete regulators (genotypes) and linear on continuous regulators (gene expression levels). The undirected line represents a multi-variate normal distribution between the relevant variables. In order to identify $A \rightarrow B$ regulation, we select either the null or the alternative hypothesis depending on the test, as shown.

Test ID	Test name	Null (hypothesis)	Alternative (hypothesis)	Selected hypothesis
0	Correlation	A B	A — B	Alternative
1	Primary (Linkage)	E A	E \rightarrow A	Alternative
2	Secondary (Linkage)	E B	E \rightarrow B	Alternative
3	(Conditional) Independence			Null
4	Relevance			Alternative
5	Controlled			Alternative

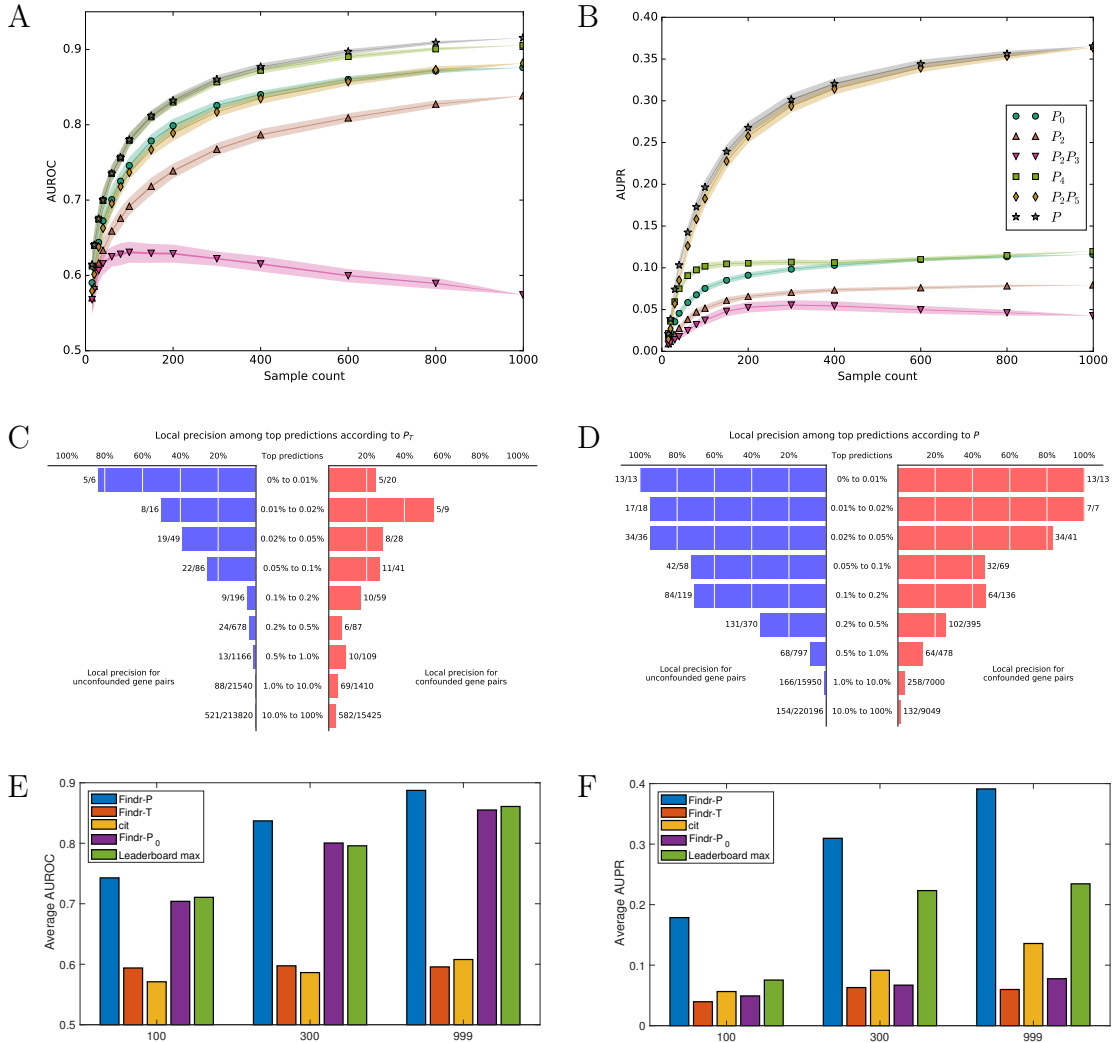


Figure 1: Findr achieves best prediction accuracy on the DREAM5 Systems Genetics Challenge. (A, B) The mean AUROC (A) and AUPR (B) on subsampled data are shown for traditional (P_2 , P_2P_3) and newly proposed (P_4 , P_2P_5 , P) causal inference tests against the baseline correlation test (P_0). Every marker corresponds to the average AUROC or AUPR at specific sample sizes. Random subsampling at every sample size was performed 100 times. Half widths of the lines and shades are the standard errors and standard deviations respectively. P_i corresponds to test i numbered in Table 1; P is the new composite test (Section 4.6). This figure is for dataset 4 of the DREAM challenge. For results on other datasets of the same challenge, see Figure S2. (C, D) Local precision of top predictions for the traditional (C) and novel (D) tests for dataset 4 of the DREAM challenge. Numbers next to each bar (x/y) indicate the number of true regulations (x) and the total number of gene pairs (y) within the respective range of prediction scores. For results on other datasets, see Figure S6. (E, F) The average AUROC (E) and AUPR (F) over 5 DREAM datasets with respectively 100, 300 and 999 samples are shown for Findr’s new (Findr- P), traditional (Findr- P_T), and correlation (Findr- P_0) tests, for CIT and for the best scores on the DREAM challenge leaderboard. For individual results on all 15 datasets, see Table S1.

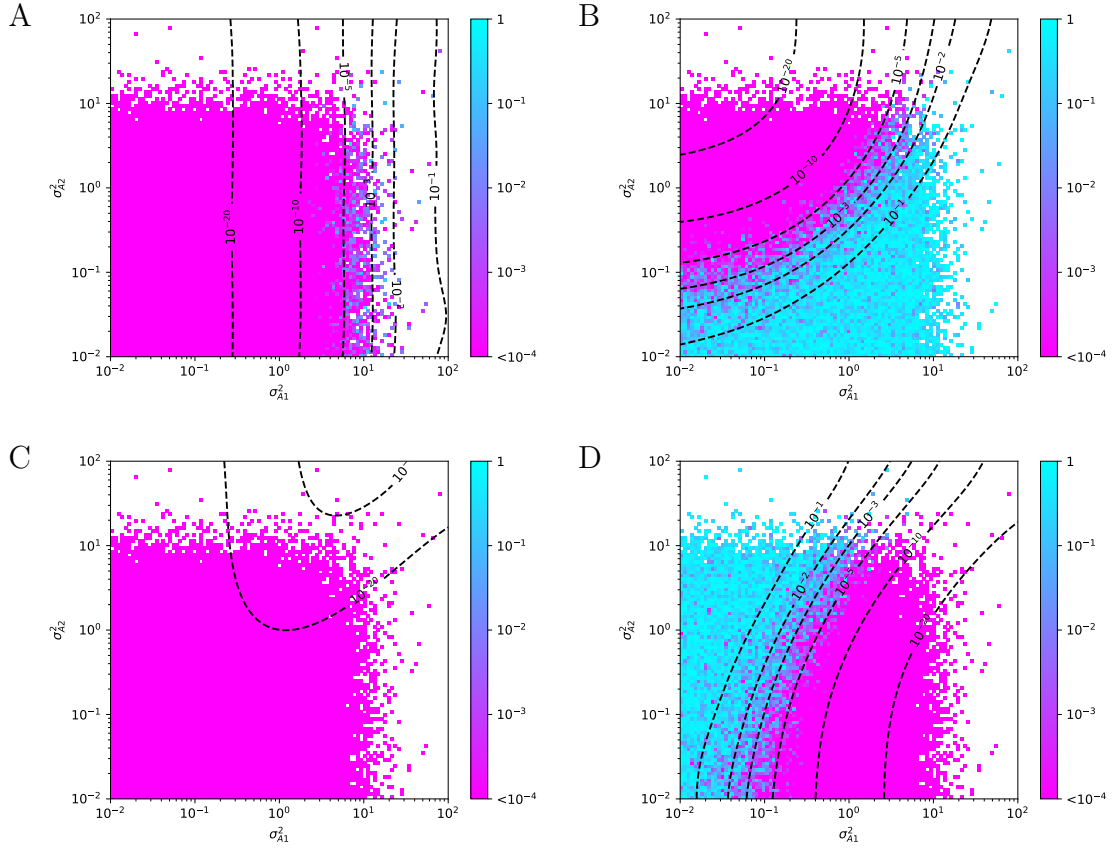


Figure 2: The conditional independence test yields false negatives for unconfounded regulations in the presence of even minor measurement errors. Null hypothesis p-values of the secondary linkage (A), conditional independence (B), relevance (C), and controlled (D) tests are shown on simulated data from the ground truth model $E \rightarrow A^{(t)} \rightarrow B$ with $A^{(t)} \rightarrow A$. $A^{(t)}$'s variance coming from E is set to one, σ_{A1}^2 is $A^{(t)}$'s variance from other sources and σ_{A2}^2 is the variance due to measurement noise. A total of 100 values from 10^{-2} to 10^2 were taken for σ_{A1}^2 and σ_{A2}^2 to form the 100×100 tiles. Tiles that did not produce a significant eQTL relation $E \rightarrow A$ with p-value $\leq 10^{-6}$ were discarded. Contour lines are for the log-average of smoothed tile values. Note that for the conditional independence test (B), the true model corresponds to the null hypothesis, i.e. small (purple) p-values correspond to false negatives, whereas for the other tests the true model corresponds to the alternative hypothesis, i.e. small (purple) p-values correspond to true positives (cf. Table 1). For details of the simulation and results from other parameter settings, see Section 4.8 and Figure S7 respectively.

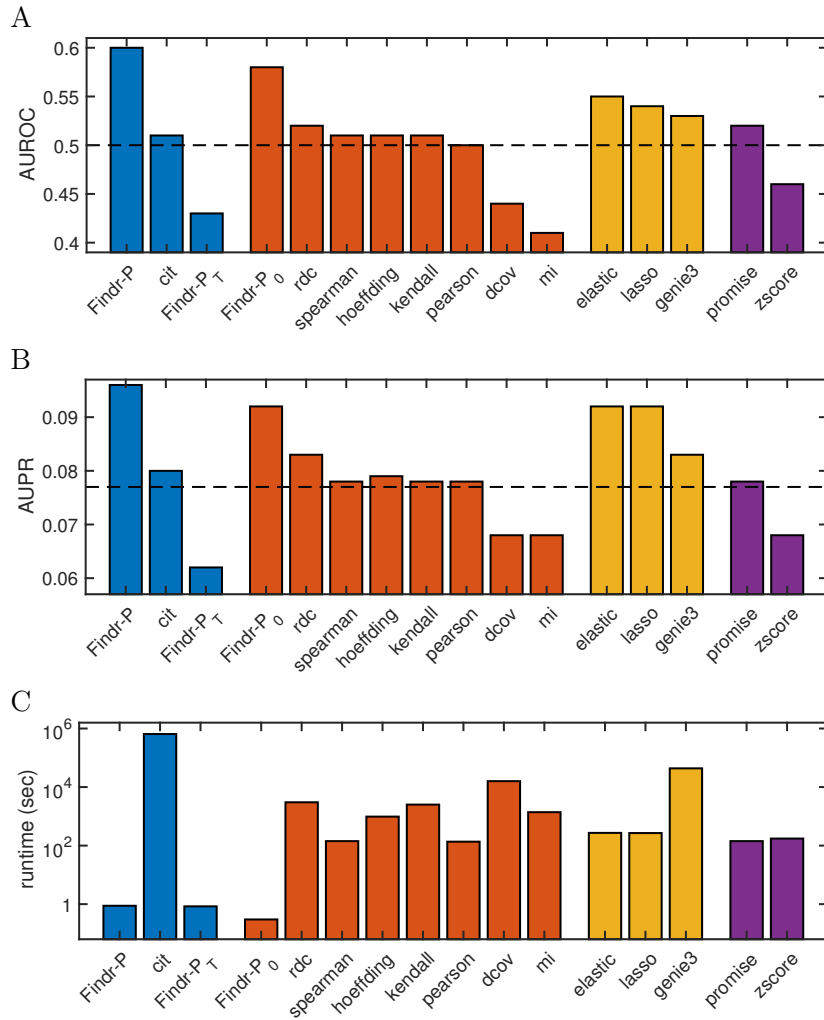


Figure 3: Findr achieves highest accuracy and speed on the prediction of miRNA target genes from the Geuvadis data. Shown are the AUROC (A), AUPR (B) and runtime (C) for 16 miRNA target prediction methods. Methods are colored by type: blue, genotype-assisted causal inference methods; red, pairwise correlation methods; yellow, multivariate regression methods; purple, other methods. Dashed lines are the AUROC and AUPR from random predictions. For method details, see Supplementary Material S2.4.

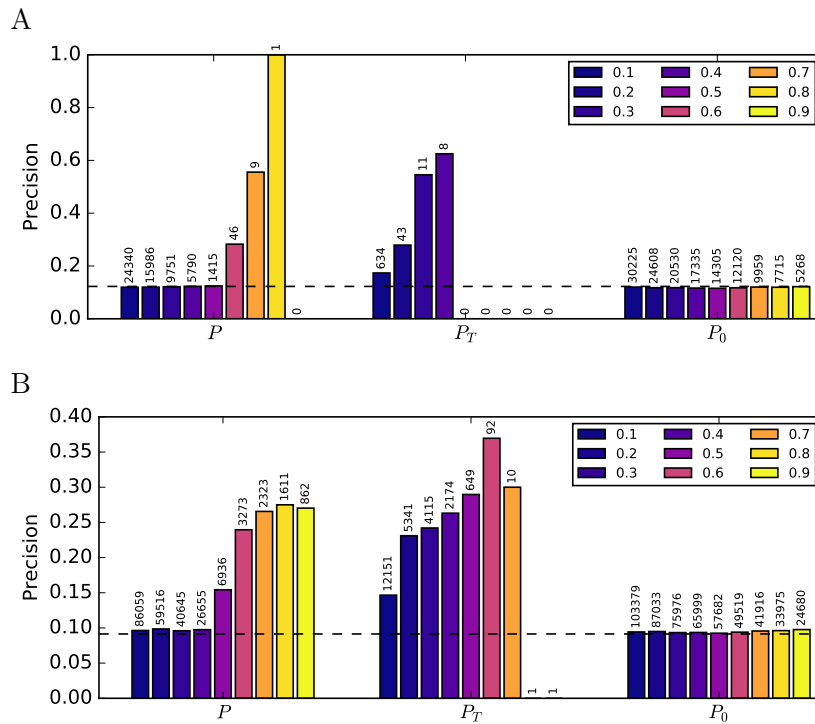


Figure 4: Findr predicts TF targets with more accurate FDR estimates from the Geuvadis data. The precision (i.e. 1-FDR) of TF target predictions is shown at probability cutoffs 0.1 to 0.9 (blue to yellow) with respect to known functional targets from siRNA silencing of 6 TFs (A) and known TF-binding targets of 20 TFs (B). The number above each bar indicates the number of predictions at the corresponding threshold. Dashed lines are precisions from random predictions.

Supplementary Material for “Efficient and accurate causal inference with hidden confounders from genome-transcriptome variation data”

Lingfei Wang and Tom Michoel[†]

Division of Genetics and Genomics, The Roslin Institute, The University of Edinburgh, Easter Bush, Midlothian EH25 9RG, UK

S1 Methods

S1.1 Practical details for Bayesian inference

In practice, real PDFs are approximated with histograms. This requires a proper choice of histogram bin widths and counts. We use $\lfloor n_p^{\frac{1}{2.5}} \rfloor$ bins, capped at 100, where n_p is the total number of points used for generating the histogram. The exponent is chosen for simultaneous precision improvements from higher bin resolution and weaker fluctuation within every bin. The bin widths are also chosen as a smooth transition from uniform sample count for every bin on the 0^+ side, to uniform bin width on the positive side. (See source code for detail.)

The bin values from real data were then postprocessed to remove empty bins that are between nonempty bins, by filling them with bin values on the positive side. We then aligned the analytical null histogram by intersecting it below the postprocessed real histogram at nonzero bin values. This obtained the ratio of null hypothesis in the mixture distribution. Bayes’ theorem then gave raw posterior probability $P(\mathcal{H}_{\text{alt}} \mid \text{LLR})$ at every bin center.

To enforce monotonicity of posterior distribution, we calculated the two following functions. First, starting from raw posterior probability $P(\mathcal{H}_{\text{alt}} \mid \text{LLR})$ at every bin center, set every the posterior at every bin to be no smaller than every value on its the negative side. Second, also starting from raw posterior distribution values $P(\mathcal{H}_{\text{alt}} \mid \text{LLR})$ at every bin center, set every the posterior at every bin to be no larger than every value on its the positive side. A mean is then taken between the two functions to ensure monotonicity whilst minimizing systematic bias.

[†]Corresponding author. Email: Tom.Michoel@roslin.ed.ac.uk

We then smoothened the monotonic posterior distribution, by convolving its bin differences against a predefined normal filter, after which cumulative sum was calculated to recover the posterior distribution. A normalization was then performed to maintain the span between the previous minimum and maximum. The major purpose of smoothening is to remove duplicate values, especially those introduced during monotonicity enforcement, rather than to obtain a visually smooth function. After smoothening, we performed linear interpolation to obtain the individual post-processed posterior probabilities for each LLR.

More details can be found in the source code.

S2 Results

S2.1 Iterative conditioning conflicts with local FDR-based probability estimation

In⁵⁵, the authors suggested that the probability of each test should be conditioned on the survival of all preceding tests, i.e. that the null distribution of each test should be estimated only on the (A, B) pairs that survive all preceding tests, although this is not implemented in Trigger package.

As an example, we applied the test combination P_2P_3 on Geuvadis dataset. After choosing an appropriate threshold probability for secondary test, as suggested in⁵⁵, we filtered only the gene pairs positive for secondary test and calculated their real and null LLR distributions of the independence test. Random permutations were applied for null distribution, with high-speed sampling from Metropolis-Hastings algorithm, whose sampling rate is exponentially increasing below secondary test’s positivity threshold, and uniformly 1 above that. To balance between efficient sampling and the prevention of being trapped in local maxima, a proper exponential factor of sampling rate ($\approx 1 - n_v/n$) can be obtained from the null LLR distribution in Eq 19.

The calculation revealed that the null and real distributions form different shapes at the $\text{LLR}^{(3)} \rightarrow 0^+$ side, which contradicted with the fundamental assumption of the local FDR-based probability estimation method (Section 4.5). On the other hand, the histograms aligned flawlessly without conditioning. We conclude that although appropriate conditioning may enhance statistical power, we are still yet to find a self-consistent approach. Since unconditioned

tests have been shown self-consistent and reliable, we do not apply test conditioning in Findr.

S2.2 Analytical null distribution matches random permutations

An important feature of Findr is the novel derivation of analytical expressions for the distributions of likelihood ratio test statistics under various null distributions (Section 4.4). We compared the analytical null distributions to empirical null distributions obtained from random simulations. Simulated data were obtained either by permuting sample labels of the independent gene (tests 0,1,2,4), or by simulating expression levels of the gene whilst taking into account existing correlations (tests 3,5). Sufficient simulated data were then fed into the original algorithm to obtain $p(\text{LLR} \mid \mathcal{H}_{\text{null}})$. As demonstrated with an example in Figure S1, our analytical derivation was confirmed indistinguishable with simulated distribution for miRNA hsa-miR-200b-3p’s targets.

More importantly, the analytical result holds for any sample size and does not assume infinite sample sizes ($n \rightarrow \infty$). Indeed, in this asymptotic limit, the LLRs of null distributions reduce to χ^2 distributions, in agreement with Wilks’s theorem⁵⁶. For example, it is easy to confirm: $\lim_{n \rightarrow \infty} 2 \text{LLR}^{(1)} \sim \chi^2(n_v - 1)$. However, approximating LLR distributions with χ^2 leads to over-estimation of the null PDF at $\text{LLR} \rightarrow 0^+$ and under-estimation at $\text{LLR} \rightarrow \infty$. The tilted $p(\text{LLR} \mid \mathcal{H}_{\text{null}})$ would then cause systematic over-estimation of $P(\mathcal{H}_{\text{alt}} \mid \text{LLR})$ for all pairs. For the Geuvadis dataset with 360 samples and $n_v = 3$, an over-estimation of $\sim 1\%$ can be observed at $\text{LLR} \rightarrow 0^+$. This counts an extra $\sim 1\%$ of all pairs as the alternative hypothesis, which can be of the same order as the actual percentage of true alternative hypotheses (typically at most a few percent).

S2.3 Subsampling and leaderboard performances of existing and new causal inference methods on DREAM datasets

DREAM challenge contains five datasets that have 999 samples. With numbering 1 to 5, they each contain different number of true regulations, from ~ 1000 to ~ 5000 incrementally, for the purpose of characterizing regulatory networks of different complexity. Performances on the fourth dataset are shown in the main article, and the rest here in Figure S2.

We compared the performances of Findr’s new test (P), Findr’s correlation test (P_0), Findr’s traditional causal inference test (P_T), and CIT on all 15 datasets against the published leaderboard of the DREAM5 Systems Genetics Challenge⁵⁷. Findr’s new test achieved highest AUROC and highest AUPR on all 15 datasets (Table S1). It is important to note that best performers can differ on different datasets or on AUROC and AUPR. For instance, the challenge winner⁵⁸ attained best AUROC on 6/15 datasets and best AUPR on 5. When compared to other inference methods that also reported improvements^{59–61}, Findr demonstrates additional virtues besides the inference accuracy. Its nonparametric nature ensures robust performances across datasets without parameter tuning. Its pairwise computation scales linearly in time with the number of regulators, targets, and samples, as opposed to multivariate regression methods, providing scalability to datasets that are orders of magnitude larger.

S2.4 Findr achieves best performance on miRNA target predictions from Geuvadis dataset

We compared the performance of Findr on miRNA target prediction from the Geuvadis dataset with a suite of network inference methods that are based on gene expression data and, for some, genotype information. They include:

- All methods in the miRLAB package⁶²:
 - Correlation methods: Pearson correlation, Spearman correlation, Kendal correlation, Distance correlation (dcov), Hoeffding’s D measure (hoeffding), Randomized Dependence Coefficient (rdc), and Mutual Information (mi).
 - Regression methods: Lasso, and Elastic-net (elastic).
 - Other methods: Z-score, and Roleswitch (promise).
 - Failed method: Intervention calculus (ida) method failed due to excessive memory usage (greater than 16GB) and hence is excluded from comparison.
- GENIE3⁶³ which utilizes random forests.
- CIT^{64,65} which performs multiple causal inference tests with genotype data.
- Multiple tests implemented in Findr, including: traditional (Findr- P_T), new (Findr- P), and correlation (Findr- P_0) tests.

The Trigger package⁵⁵ was not attempted because its eQTLs discovery routine exceeds both our memory and time limitations.

Their AUROCs, AUPRs, and running times are presented in Table S2. The ROC and PR curves are shown in Figure S8. We observed the following results:

- The correlation test topped among methods without genotype information, and in particular performs much better than Pearson and Spearman correlations. The performance gain is due to Bayesian inference, which is able to account for different gene roles such as hubs. This suggests the possibility of replacing correlation based methods with their FPR estimation counterparts in future inference of genetic regulations.
- The new test P performed better than correlation test P_0 . This is the first comparative study to demonstrate the effect of genotype information in the inference of gene regulatory relations.
- The traditional causal inference test performed worse than random predictions. This confirms with real data that the indirect secondary test fails to identify true but weak regulations. The independence test had negligible effect as the sample size is small (not shown in Figure S8).
- Findr achieved higher AUROC and AUPR than all other methods attempted. It was also much faster than all other methods, especially CIT which also includes genotype data.
- Findr obtained a lower precision than lasso and elastic-net at small recalls. This might be explained by the fact that lasso and elastic-net are multi-variate methods which incorporate all other gene expression levels besides pairwise information, and therefore exclude indirect regulators better.

S2.5 Findr predicts transcription factor targets with accurate FDR estimates

Since CIT is much slower than Findr, with CIT we were only able to infer genetic regulations of the intersection set of the prediction and groundtruth datasets, as opposed to inferring all possible regulations with Findr.

As shown in Figure 4, AUPRs and AUROCs for TF target prediction with respect to known targets from siRNA silencing or TF-binding did not exhibit substantial differences, other than modest improvement over random predictions. We believe this is due to the unavoidable noise and size limitations in groundtruth data, which lead to large fluctuations in evaluation metrics and therefore could not compare methods perfectly. Furthermore, AUPR and AUROC test the entire ranked list of predictions for overlap with the groundtruth and will miss differences in enrichment for true positives between methods if they occur only among a small fraction of top-ranked predictions.

The construction of gold standard regulatory networks from TF-binding data is dependent on how TF binding sites are mapped to target genes. Here a TF regulatory interaction was assumed if a gene had at least two binding sites for a particular TF within 10kb of its transcription start site (TSS)⁶⁶. We repeated the analysis using the high-confidence (binding within 2.5kb) TF-target network derived from ENCODE from ChIP-sequencing data of 119 TFs in five cell types, including the lymphoblastoid cell line GM12787⁶⁷. Fourteen TFs had a significant eQTL in the Geuvadis data. The analysis results are consistent (Figure 4 and Figure S10).

S3 Discussion

- Existing softwares/methods not considered in this study:

No previous causal inference software has been able to handle the size of modern datasets. In Trigger⁵⁵, eQTL discovery and causal inference are inextricably linked, which is impractical for any sizeable dataset, especially for mammalian species; much more efficient tools for eQTL discovery have meanwhile become available^{68,69}. NEO⁷⁰ is similar to CIT⁶⁵ in the tests employed, but even slower. It is able to account for multiple eQTLs, but avoids permutations using asymptotic χ^2 approximations, which result in deflated estimations for null distributions as shown in Section S2.2. As stated in the discussion, multi-variate network inference can be a downstream analysis based on pairwise causal inference, but evaluating such methods⁷¹⁻⁷³ fell out of the scope of this paper. Finally, note that CIT computes null distributions by permutation, separately for every gene pair, requiring months to tens of years of CPU time on a modern dataset. We

were only able to include comparisons to CIT on the Geuvadis data by limiting it to the subset of gene pairs in the ground-truth tables, which correspond to 0.2% of all gene pairs for the TF target prediction case.

- Considerations on human datasets:

Proving in an easily reproducible manner that the results on simulated DREAM data also hold on human data is challenging, due to the often restricted access to individual-level genotype data and the limited availability of reference databases of known interactions, especially when cell type specificity is taken into account. We performed our evaluation on the Geuvadis data, which provides transcriptome data in lymphoblastoid cells of nearly 400 individuals whose genotype data is publicly available through the 1000 Genomes project. We found that Findr predicted miRNA targets more accurately than other causal inference methods and a panel of machine learning methods that used expression data alone. Although the absolute power to predict miRNA targets may appear modest, we were primarily interested in the relative performance of various methods, and did not incorporate information about known miRNA biology, such as a preference for negative correlations or the presence of miRNA seed sequences. Moreover, since miRNAs are frequently studied in the context of diseases such as cancer, the ground-truth set of experimentally confirmed targets may represent a biased set of interactions that are not necessarily present in the lymphoblastoid cell type studied.

To address the issue of cell type specificity, we analysed the predicted targets of 25 transcription factors for which either functional targets from siRNA silencing experiments or DNA-binding targets from ChIP-sequencing or DNase footprinting in lymphoblastoid cells were available. For both data types we found that Findr’s new test achieved a 2 to 5-fold enrichment for known TF targets compared to using TF-target coexpression alone, showing that causal inference is indeed able to prioritize highly probable causal interactions among coexpressed genes. Although Findr’s new test and conditional independence based causal inference tests resulted in similar performances in this case, the estimated FDRs of the traditional method were greatly inflated, such that enrichment for known interactions was only observed at estimated local FDR $>40\%$. This reaffirms the finding, consistently observed in all our analyses, that the conditional-independence

methods are over conservative for calling causal interactions in the context of complex regulatory networks.

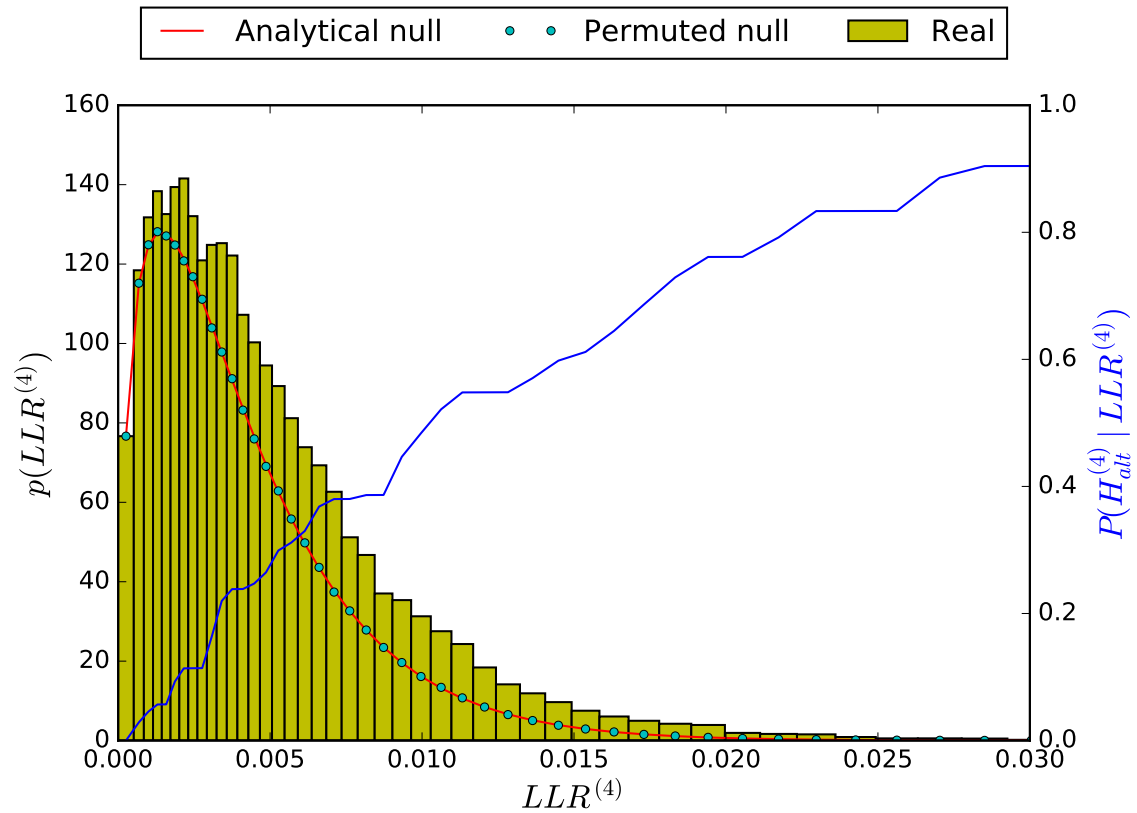


Figure S1: LLR distributions of the relevance test for hsa-miR-200b-3p on 23722 potential targets of Geuvadis dataset. Real, analytical null, and permuted null distributions are demonstrated in the figure, together with the curve of inferred posterior probability of alternative hypothesis. Permutations were randomly conducted on all potential target genes for 100 times. The alignment between analytical and permuted null distributions and the consistent incremental trend of posterior probability verify our method in deriving analytical null distributions.

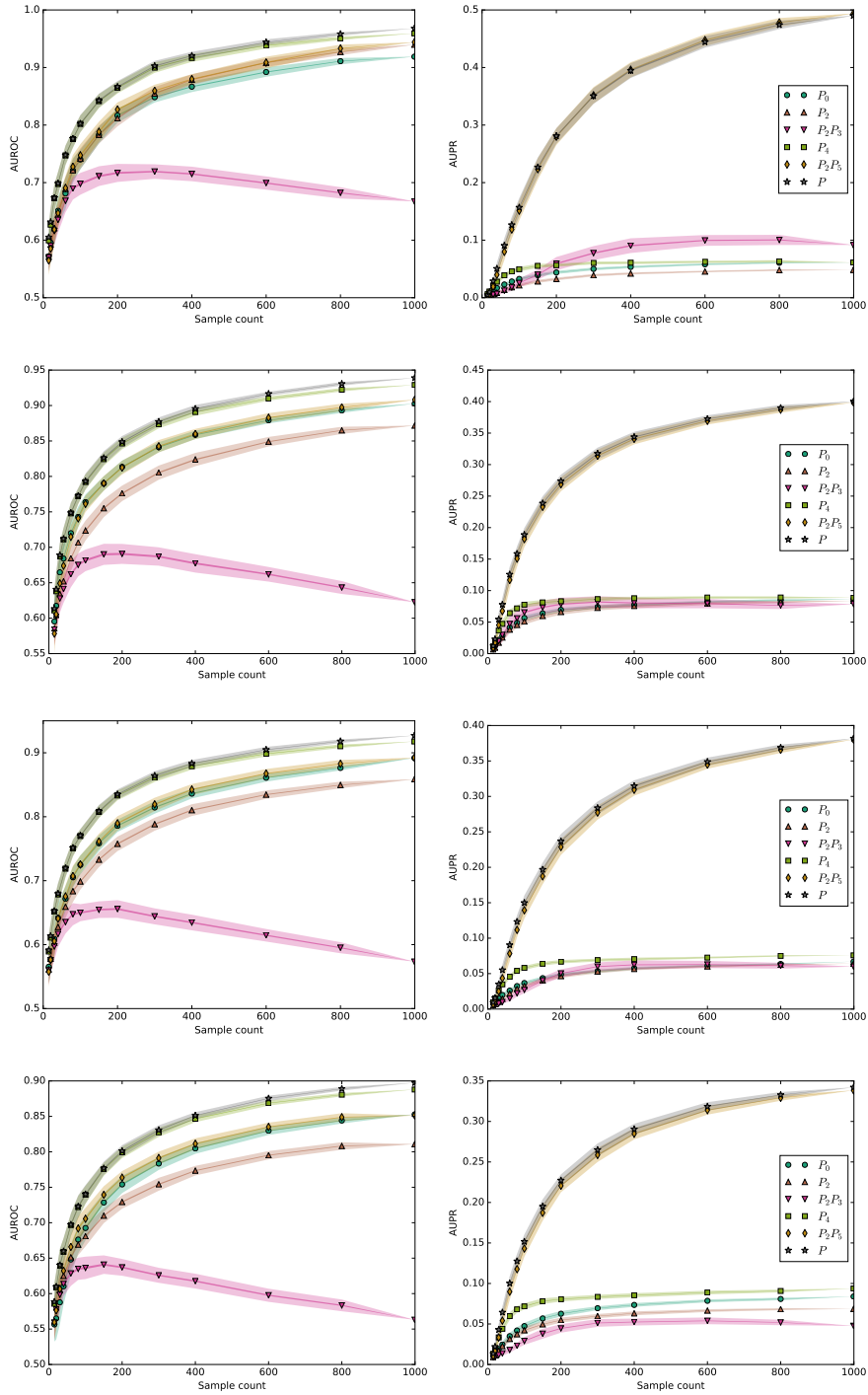


Figure S2: The mean AUROC and AUPR on subsampled data are shown for causal inference with traditional and new tests, together with the baseline correlation test. Every marker corresponds to the average AUROC or AUPR at specific sample sizes. At every sample size we performed 100 subsampling. Half widths of the lines and shades are the standard errors and standard deviations respectively, of AUROC or AUPR. Figures from top to bottom correspond to datasets 1, 2, 3, 5. For dataset 4, see Figure 1.

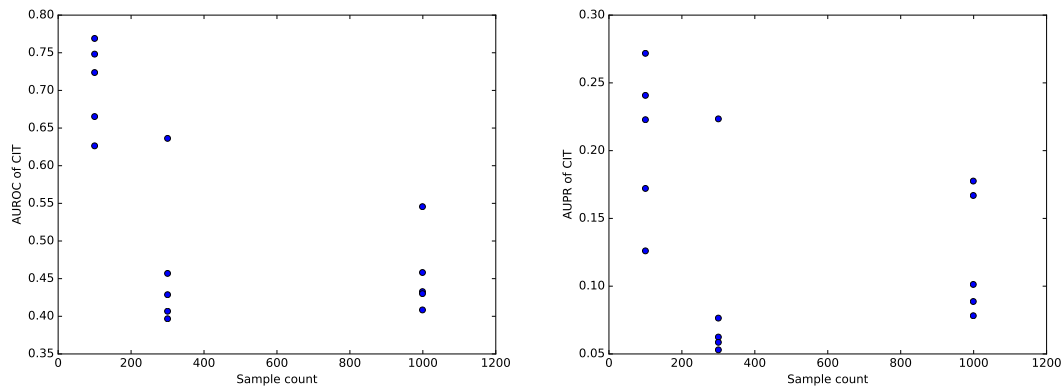


Figure S3: The AUROC and AUPR of CIT⁶⁵ are shown for all 15 datasets of DREAM challenge. Every marker corresponds to the AUROC or AUPR of one dataset. CIT is an R package that includes the conditional independence test, along with tests 2 and 5, while also comparing $E \rightarrow A \rightarrow B$ against $E \rightarrow B \rightarrow A$. The subsampling analysis on CIT was not feasible due to its low speed.

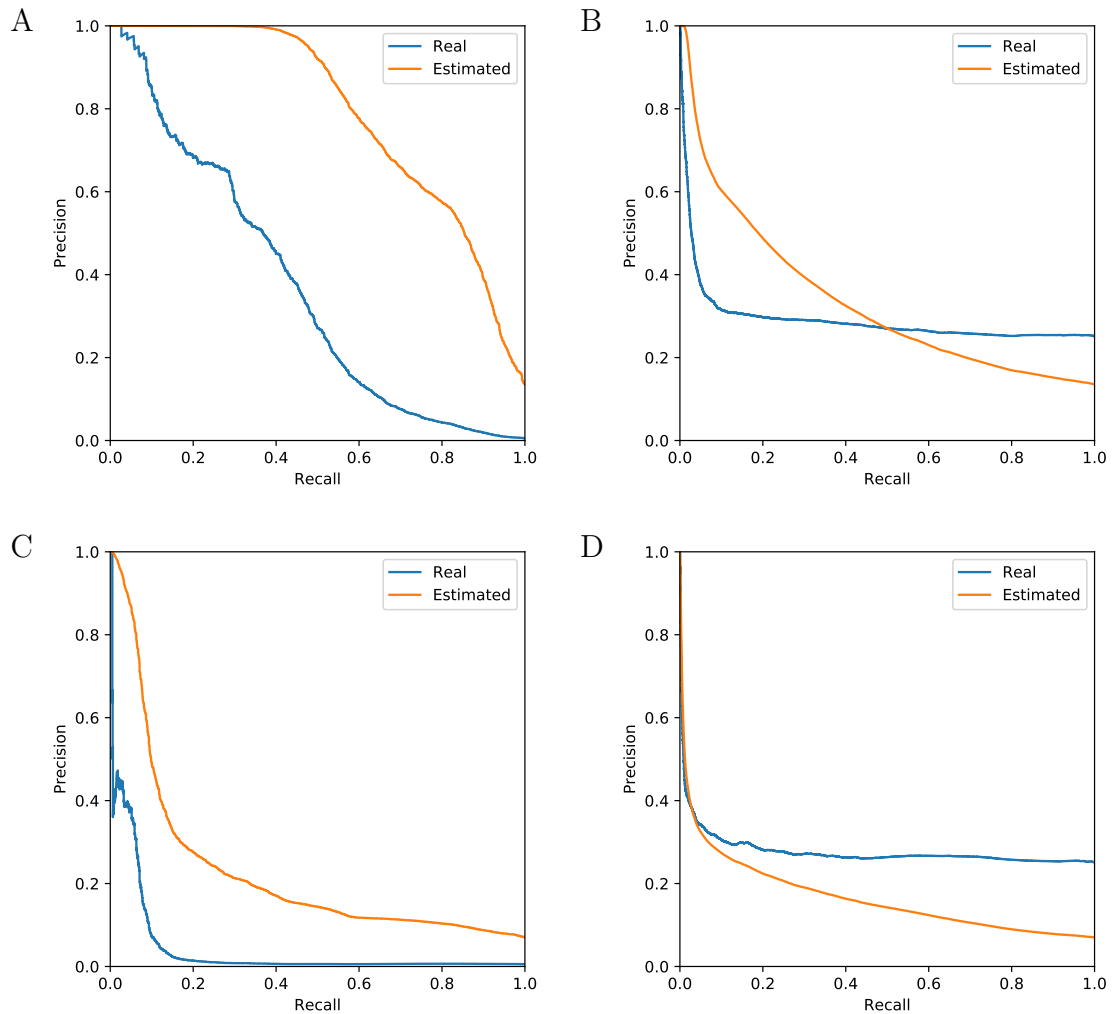
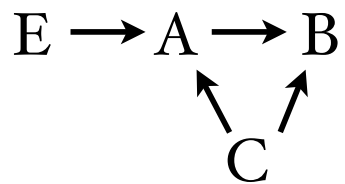
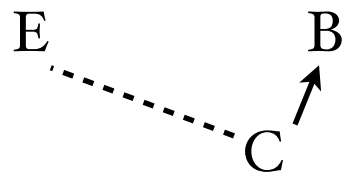


Figure S4: Estimated and real precision-recall curves for dataset 4 of the DREAM challenge. The real precision was computed according to the groundtruth, whilst the estimated precision was obtained from the estimated FDR from the respective inference method (precision = $1 - \text{FDR}$). Only genes with cis-eQTLs were considered as primary targets in prediction and validation. Both the novel (A, B) and the traditional (C, D) tests were evaluated. In A, C the original groundtruth table was used to validate predictions, whereas in B, D an extended groundtruth was used that also included indirect regulations at any level based on the original groundtruth.



(a) With confounder before conditioning on A



(b) With confounder after conditioning on A

Figure S5: The conditional independence test fails in the presence of hidden confounders. When A and B are both regulated by a hidden confounder C , which is independent of E (left), A becomes a collider and conditioning on A would introduce inter-dependency between E and C , which maintains $E \rightarrow B$ regulation (right).

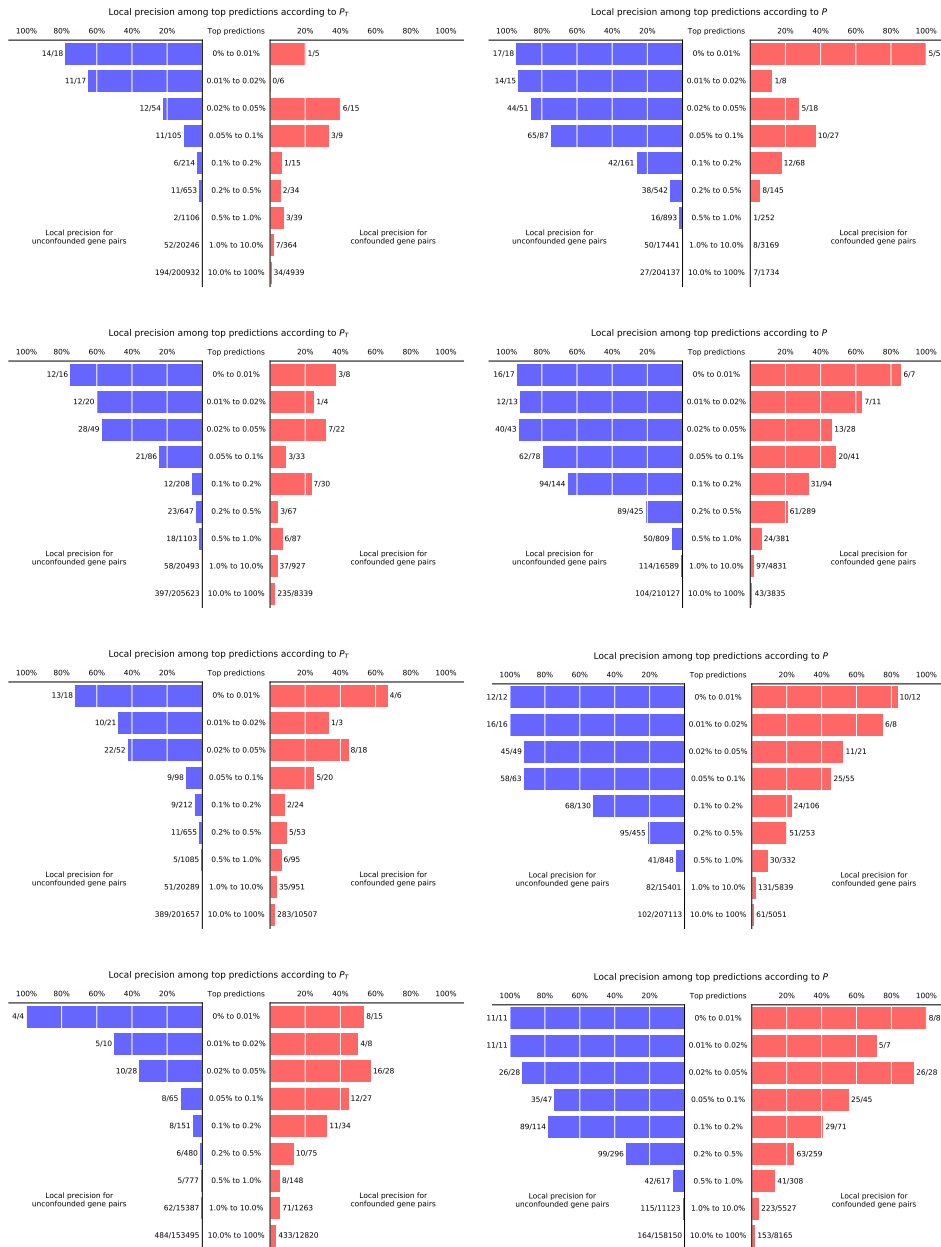


Figure S6: Local precision of top predictions for the traditional (left) and novel (right) tests for datasets (top to bottom) 1, 2, 3, and 5 of the DREAM challenge.

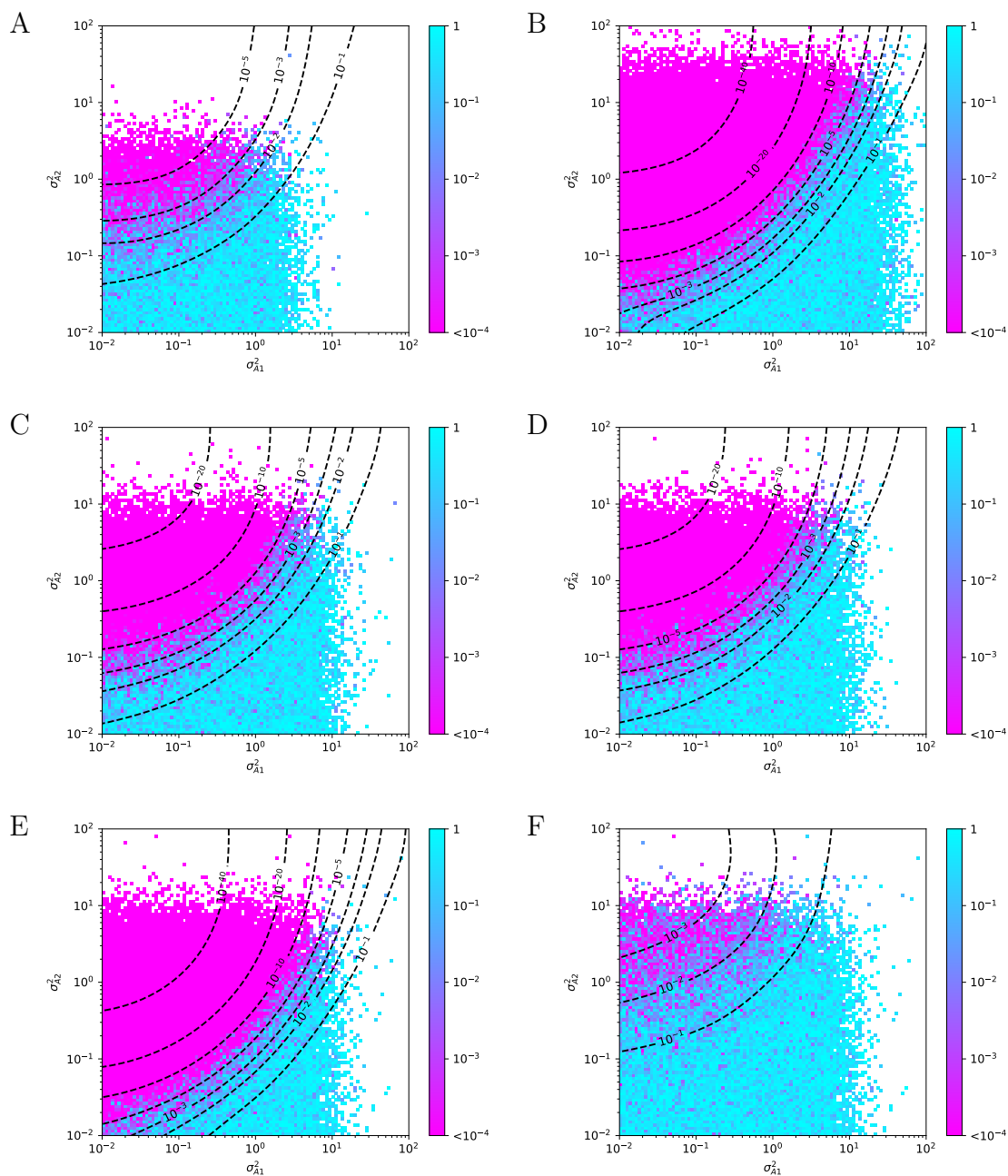


Figure S7: Null hypothesis p-values of the conditional independence test on simulated data from the ground truth model $E \rightarrow A^{(t)} \rightarrow B$ with $A^{(t)} \rightarrow A$ under parameter settings other than Figure 2. (A,B) 100 (A) or 999 (B) samples. (C,D) Minor allele frequency is 0.05 (C) or 0.3 (D). (E,F) Regarding B 's variance from $A^{(t)} \rightarrow B$ as unit variance, B 's variance from other sources including measurement errors is 0.2 (E) or 20 (F). Unmentioned parameters remain the same as in Figure 2.

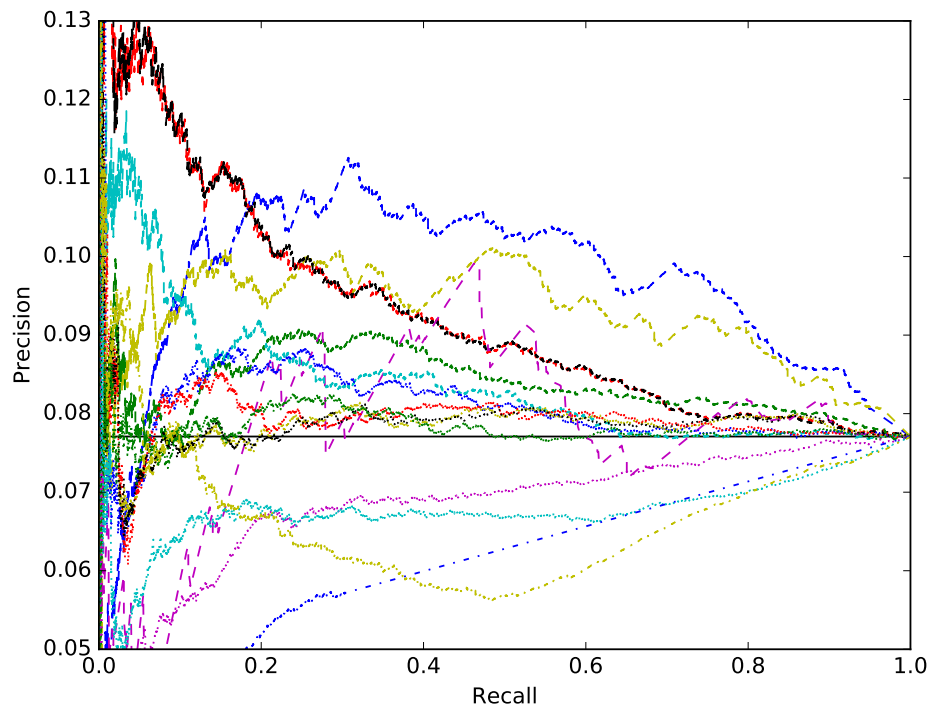
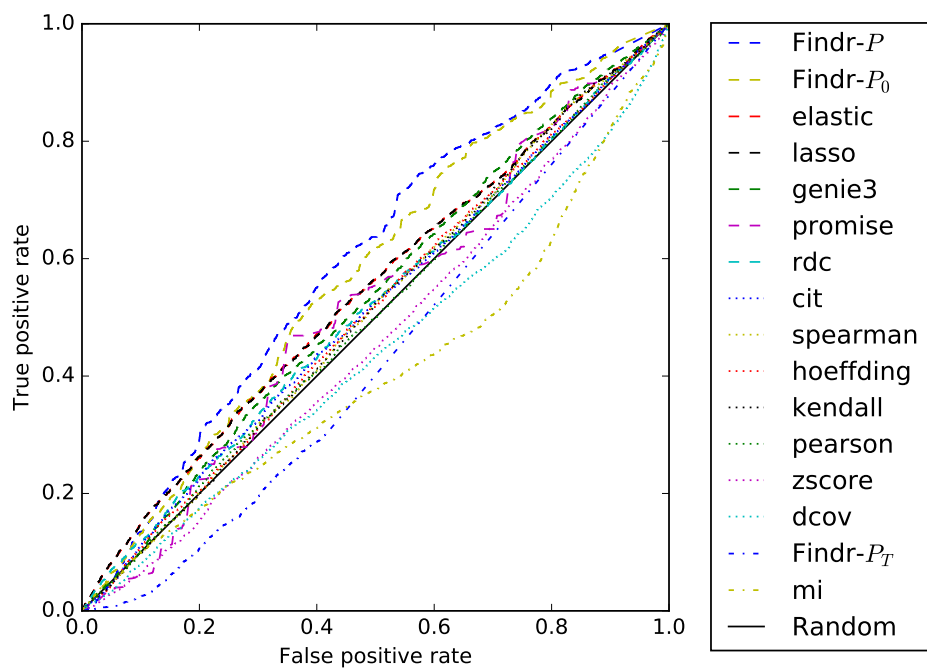


Figure S8: ROC (top) and PR (bottom) curves of miRNA target predictions were compared for Findr’s traditional, new, and correlation tests, GENIE3, CIT, and 11 methods in miRLAB, based on Geuvadis data. The solid black lines correspond to expected performances from random predictions. A higher curve indicates better prediction performance.

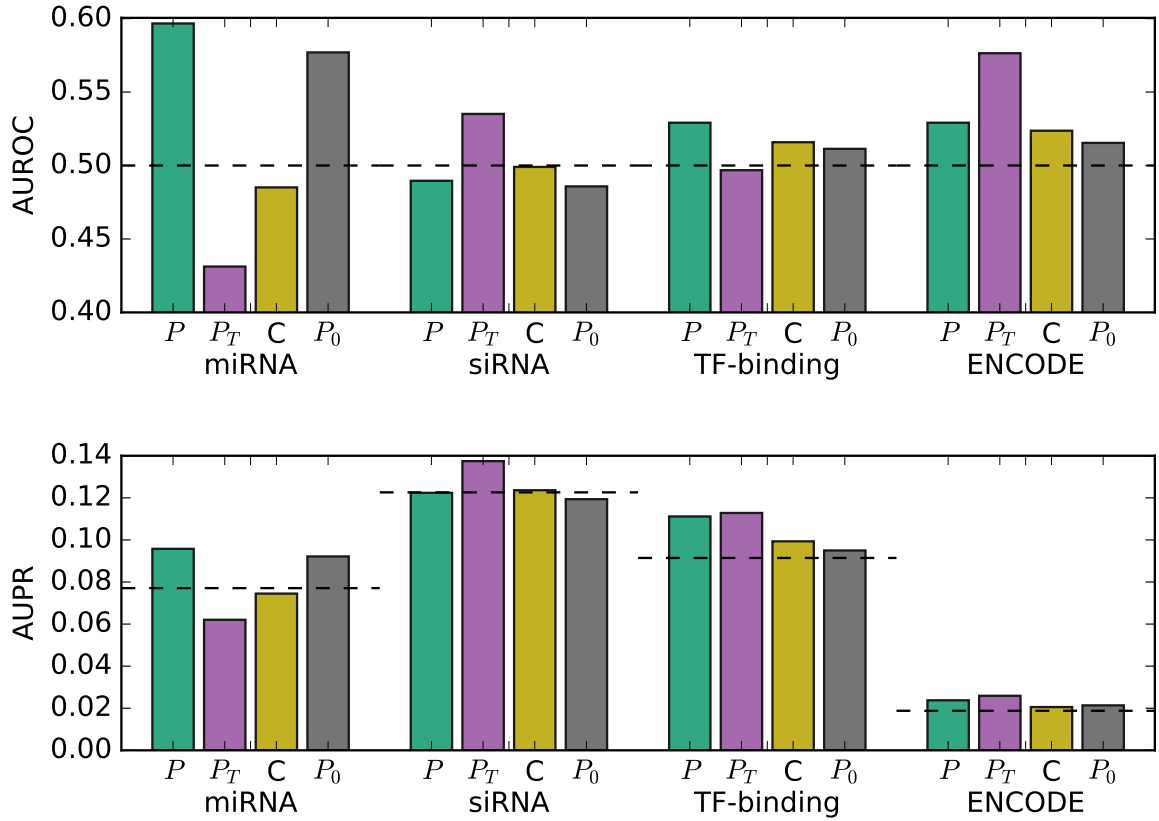


Figure S9: Three methods of causal inference were evaluated and compared against the baseline correlation test method (P_0): Findr's new test (P), traditional causal inference test in Findr (P_T), and CIT (C). AUROC and AUPR metrics are measured for three inference tasks (Section 4.1). MiRNA compares miRNA target predictions based on Geuvadis miRNA and mRNA expression levels against groundtruths from miRLAB. SiRNA and TF-binding compares gene-gene interaction predictions based on Geuvadis gene expression levels against groundtruths from siRNA silencing and TF-binding measurements⁶⁶ respectively. ENCODE compares the same gene-gene interaction predictions against TF-binding networks derived from ENCODE data⁶⁷. Dashed lines indicate expected performances from random predictions.

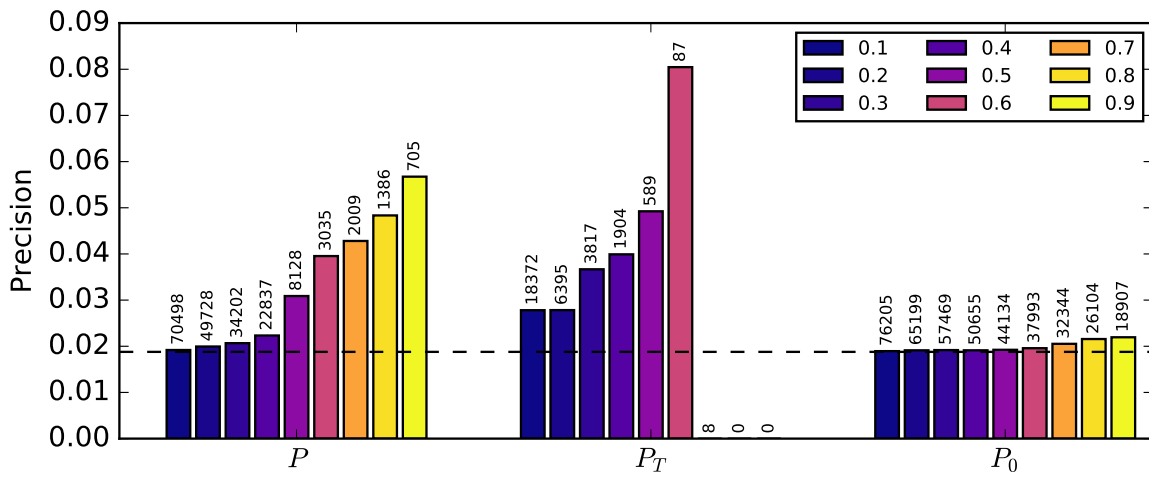


Figure S10: Inference precision at estimated precision cutoffs 0.1 to 0.9 with respect to groundtruth network derived from TF binding of 14 TFs from ENCODE data⁶⁷. The number above each bar indicates the number of positive predictions at the corresponding threshold. The dashed line is precision from random predictions.

Table S1: Predictions from Findr’s new (P), traditional (P_T), and correlation (P_0) tests, and CIT were compared against DREAM challenge leaders on AUROC and AUPR for all 15 DREAM datasets. All cis- and trans-genes are included. DREAM challenge constrained the maximum number of submitted regulations by 100,000, which were also applied in our evaluation. Findr’s new test consistently obtained higher AUROC and AUPR than all other methods, including the leaders of DREAM challenge.

Sample count	100 samples					300 samples					999 samples				
	1	2	3	4	5	1	2	3	4	5	1	2	3	4	5
Test id															
P AUROC	0.772	0.750	0.737	0.736	0.719	0.882	0.842	0.839	0.825	0.797	0.941	0.899	0.882	0.867	0.848
P_T AUROC	0.617	0.609	0.597	0.574	0.572	0.647	0.594	0.581	0.592	0.573	0.616	0.611	0.570	0.616	0.565
P_0 AUROC	0.709	0.706	0.706	0.699	0.700	0.843	0.798	0.803	0.792	0.766	0.905	0.870	0.850	0.837	0.813
CIT AUROC	0.585	0.582	0.571	0.548	0.569	0.630	0.586	0.575	0.574	0.566	0.614	0.640	0.594	0.614	0.577
Leader AUROC	0.754	0.718	0.699	0.694	0.688	0.861	0.793	0.799	0.769	0.757	0.933	0.885	0.845	0.828	0.813
P AUPR	0.222	0.183	0.172	0.161	0.155	0.421	0.326	0.279	0.264	0.258	0.547	0.368	0.366	0.342	0.333
P_T AUPR	0.044	0.048	0.042	0.023	0.041	0.109	0.054	0.051	0.054	0.047	0.070	0.068	0.042	0.070	0.049
P_0 AUPR	0.051	0.049	0.040	0.051	0.055	0.084	0.053	0.063	0.078	0.057	0.093	0.072	0.070	0.076	0.077
CIT AUPR	0.075	0.066	0.060	0.031	0.050	0.162	0.075	0.074	0.080	0.067	0.168	0.149	0.098	0.168	0.096
Leader AUPR	0.103	0.072	0.067	0.068	0.067	0.309	0.243	0.191	0.182	0.191	0.358	0.258	0.195	0.183	0.178

Table S2: AUROCs and AUPRs of miRNA target predictions were compared for Findr’s traditional, new, and correlation tests, GENIE3, CIT, and 11 methods in miRLAB, based on Geuvadis data. Higher AUROC and AUPR values signify stronger predictive power. Program running times have units in seconds (s), minutes (m), hours (h), or days (d). Findr outperformed other methods in statistical power and speed, with or without genotype information.

	Findr- P	Findr- P_0	elastic	lasso	genie3	promise
AUROC	0.60	0.58	0.55	0.54	0.53	0.52
AUPR	0.096	0.092	0.092	0.092	0.083	0.078
Time	0.88s	0.30s	4.53m	4.47m	12.1h	2.37m
	rdc	cit	spearman	hoeffding	kendall	pearson
AUROC	0.52	0.51	0.51	0.51	0.51	0.50
AUPR	0.083	0.080	0.078	0.079	0.078	0.078
Time	50.3m	7.5d	2.37m	16.3m	41.9m	2.27m
	random	zscore	dcov	Findr- P_T	mi	
AUROC	0.50	0.46	0.44	0.43	0.41	
AUPR	0.077	0.068	0.068	0.062	0.068	
Time	-	2.90m	4.42h	0.84s	23.1m	